THE UNIVERSITY OF MICHIGAN
COLLEGE OF ENGINEERING
Department of Meteorology and Oceanography

Technical Report

ADDITIONAL RESULTS FROM MULTI-LAYER CALCULATIONS OF ATMOSPHERIC DIABATIC PROCESSES AND THE GENERATION OF AVAILABLE POTENTIAL ENERGY

George E. Lawniczak, Jr.

Aksel C. Wiin-Nielsen
Project Director

ORA Project 00263

supported by:

NATIONAL SCIENCE FOUNDATION
GRANT NO. GA-16166
WASHINGTON, D.C.

administered through:

OFFICE OF RESEARCH ADMINISTRATION ANN ARBOR

December 1970

ACKNOWLEDGMENTS

I am particularly indebted to my friend, Professor Aksel Wiin-Nielsen, for his guidance and assistance throughout this study. Personal conversations in Ann Arbor and Copenhagen or phone calls have never failed to provide me with a fresh outlook and renewed spirit.

I wish also to thank the Office of Research Administration at The University of Michigan for aid in preparing this report, particularly Mary L. Falcone. All computations were performed on the IBM-360 system at the University and I am indebted to those unsung heroes, the maintenance technicians.

ABSTRACT

This report covers the results obtained from a continuation of a study described in the author's doctoral thesis (1969). Using Lorenz' (1955) definitions, calculations of the generation of available potential energy (APE) are made.

The data are the daily objective height analyses for the Northern Hemisphere from the Navy's Fleet Numerical Weather Central (FNWC) Monterey, California, for January 1969. (FNWC's numerical grid contains the equator as an inscribed circle.) A five-layer quasi-geostrophic model is used to compute the net effect of the diabatic processes in each layer within the volume between 100 and 30 cb. Diabatic effects are calculated using lower boundary computations and the accumulated vertical changes in the total derivative (horizontal) of the geostrophic potential vorticity. Static stability is assumed to be linearly pressure dependent and variable terrain height and surface frictional effects are included.

Because of the failure of geostrophic theory in the high troposphere and above, and due to the data coverage, only the results in about 30% of the earth's atmosphere can be discussed. However, previous studies have indicated that exclusion of the stratosphere is not significant.

The monthly mean average of the diabatic processes indicates that the surface effects of permanent snow or ice cover are felt throughout the troposphere. Net heating and cooling regions are separated near 50N and this separation extends almost vertically to 30 cb. The maximum net heating (cooling) occurred near 42N (65N). Polar front processes are responsible for the heating maximum and polar night conditions produce the cooling maximum. Results for the layers centered at 45 and 35 cb indicate that average high cloudiness is effective in trapping long wave-radiation, producing average net heating areas.

Using the daily values of the diabatic effects in the troposphere for January 1969, the average generation of zonal APE was 55×10^{-4} kj m^{-2} sec^{-1} and eddy APE was destroyed at the rate of 29×10^{-4} kj m^{-2} sec^{-1}. Therefore, on the average, heating (cooling) occurred in the low (high) latitudes and the warm (cold) eddies were cooled (heated) during this month.

In the region analyzed, most of the generation and destruction occurred in the lowest 30 cb of the atmosphere. Polar latitudes contributed most to the generation of zonal APE while baroclinic activity associated with the polar front led to the maximum destruction of eddy APE near 40N.

Harmonic analysis reveals that the long and medium waves were most important in destroying eddy APE. Waves 1 and 4 were the dominant destructive modes.

TABLE OF CONTENTS

TABLE OF CONTENTS (Concluded)

LIST OF TABLES

LIST OF FIGURES

LIST OF FIGURES (Concluded)

LIST OF SYMBOLS

a = mean radius of the earth

c_p = specific heat of air at constant pressure

d = distance between horizontal grid points

e = eddy parameter when used as a subscript

f = Coriolis parameter, $2\Omega\sin\varphi$

$\bar{f}$ = value of the Coriolis parameter at 45N

g = acceleration of gravity

i = pressure layer counter in (2.30), (2.31), (2.22)

i = grid-point counter in the x-direction in Appendix

$\vec{i}$ = unit horizontal vector pointing toward the east

j = latitude band counter in (2.30), (2.31)

j = grid-point counter in the y-direction in Appendix

$\vec{j}$ = unit horizontal vector pointing toward the north

k = number of latitude bands in (2.30), (2.31)

$\vec{k}$ = unit vertical vector pointing upward

m = meters when used in units specifications

m = number of pressure layers in (2.30), (2.31)

m = map factor in Appendix, $(\frac{1.86603}{1 + \sin\varphi})$

n = wave number when used as a subscript

o = lower boundary parameter when used as a subscript

p = pressure

$\bar{p}$ = 100 cb

t = time

u = component of speed along the x axis

v = component of speed along the y axis

x = distance coordinate increasing toward the east

y = distance coordinate increasing toward the north

y = Fourier coefficient in (2.30), (2.31)

z = height above mean sea level

z = a zonal parameter when used as a subscript

z = Fourier coefficient in (2.30), (2.31)

A = available potential energy

APE = available potential energy

B = integrand of (2.8)

C_D = drag coefficient

D = departure value

E = eddy parameter when used as a subscript

F_x = horizontal component of friction force per unit mass in the x-direction

F_y = horizontal component of friction force per unit mass in the y-direction

G = generation of available potential energy

H = diabatic processes per unit mass and unit time

I = internal energy

K = kinetic energy

N = total number of harmonic components considered in (2.31)

P = potential energy

R = gas constant for air

S = surface area

ST = specific temperature anomaly in Appendix

T = temperature

$\vec{V}_o$ = geostrophic surface wind vector

$\vec{V}$ = horizontal geostrophic wind vector

Y = Fourier coefficient in (2.30), (2.31)

Z = Fourier coefficient in (2.30), (2.31)

Z_p = standard height of a given pressure level

α = specific volume

ζ = vertical component of relative vorticity

θ = potential temperature

λ = longitude

ξ = geostrophic potential vorticity

ρ = density

σ = a measure of static stability

τ_x = horizontal component of frictional stress acting in the x-direction

τ_y = horizontal component of frictional stress acting in the y-direction

φ = latitude

ω = dp/dt

Δ = a difference operator

Φ = gz, the geopotential

$\nabla = \partial/\partial x \, \vec{i} + \partial/\partial y \, \vec{j}$

$\nabla^2 = \partial^2/\partial x^2 + \partial^2/\partial y^2$

$'$ = deviation from area mean value

CHAPTER 1

ENERGETICS AND AVAILABLE POTENTIAL ENERGY

1.1. INTRODUCTION

The concept of energy describes the ability of an object or a system to do work, i.e., to exert a force through a distance. Studies of the energetics of the earth's atmosphere are intended to show how the atmosphere works by determining the energy flows among the various energetical forms. Energy forms which are significant within the atmosphere consist of three distinct types: (1) kinetic energy, (2) potential energy, and (3) internal energy.

Kinetic energy is the measure of work that a moving object can perform in being slowed to a state of rest. An example is the energy the wind expends as it propels a sailboat. Obviously the faster a particle moves the more kinetic energy it has.

Potential energy defines the capability of doing work by virtue of an object's position in an external force field. A mass at a greater distance from the center of the force field has more potential energy. Matter falling due to the force of a gravitational field is an example of a body losing this form of energy.

Internal energy may be defined as the sum of the electromagnetic potential energy of electrons, nuclei, and the molecules of matter and the kinetic energy due to the molecular motions. This energy is closely associated with the average energy of the thermal motions of molecules, i.e., the temperature of an object. When two identical objects with different temperatures are placed in

contact, the warmer mass transfers internal energy to the cooler body through molecular collisions until both objects have the same temperature or internal energy.

Energy is important because all matter possesses it and because energy is a conserved property, i.e., it can be neither created nor destroyed but only transformed from one form to another or transferred to another system. Thus a system in isolation from the rest of the universe acts under the constraints of conservation of energy. Since the earth-atmosphere system shows no tendencies for velocity and temperature changes over a long time it can be considered to be an isolated system. This means that over a sufficiently long time the system must be in equilibrium with the environment. Since the system interacts with its environment only through radiational processes, insolational warming received from the sun must be balanced by a cooling loss through long wave emission. However these relationships are valid only over a long time. Substantial departures from equilibrium may exist for short periods.

Energy studies based on atmospheric observations must employ the hydrostatic assumption. This is true because the assumption is used in calculating these atmospheric data. The hydrostatic assumption states that the upward-directed component of the pressure gradient force is balanced by the downward-acting acceleration of gravity at all times throughout the atmosphere. A direct consequence of this assumption is that the vertical velocity of the system is not a free variable but must be determined from the other state parameters. Since the resulting vertical velocities required to maintain the balance are small the flow within the atmosphere can be considered to be basically horizont

Within an hydrostatic atmosphere, Haurwitz (1941) has shown that the potential and internal energy of a column are proportional. That is, an increase of one requires an increase in the other. Therefore it is convenient to combine potential and internal energy into one form. Total potential energy is the name given to the sum of these components in an hydrostatic atmosphere. Wiin-Nielsen (1968) shows that the energy flow for an atmosphere exhibiting this equilibrium can be displayed as in the upper diagram of Fig. 1. Here G(I) represents the generation of internal energy; $C(I,K_H)$ signifies the conversion of internal energy into the kinetic energy of the horizontal flow; C(I,P) portrays the relationship between internal and potential energy; $D(K_H)$ denotes the dissipation by friction of the kinetic energy of the horizontal flow. The direction of the arrows is determined by noting that over a sufficient time period the generation and conversion terms must off-set the removal of kinetic energy since the winds do not ultimately cease to blow.

Another useful approximation available to the investigator is the quasi-geostrophic theory. Charney (1948) provided a system by which the magnitudes of the terms in the hydrodynamical equations could be compared through the use of nondimensional analysis. He formulated the results for the synoptic weather scale while Burger (1958) extended this concept to the planetary waves. The approximation consists of keeping only the terms of largest comparable magnitude. It gets its name because the geostrophic wind relationship is the resultant when the largest terms are retained in the first two equations of motion. Use of the theory is made after the vorticity equation is formed by cross-differentiating the first two equations of motion and subtracting. The geostrophic

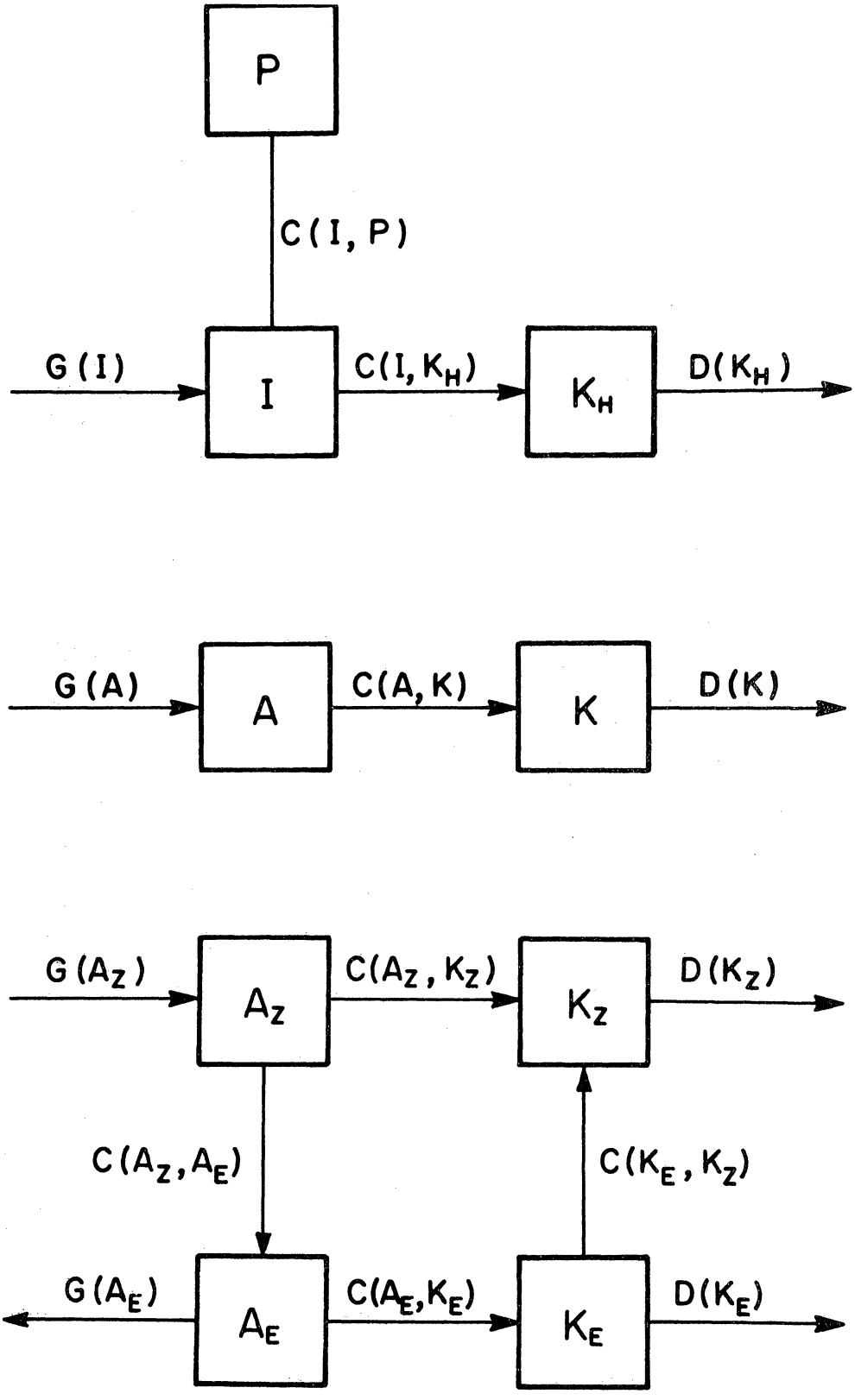

Fig. 1. Flow diagrams of energy for an atmosphere in hydrostatic equilibrium.

wind is not used in the divergence term in the vorticity equation and hence the "quasi" portion of the name. Results of numerical forecasts using the theory led to the problem of spurious anticyclogenesis. This is due to the divergent nature of the geostrophic wind where southerly flow is convergent and northerly flow is divergent. This pattern does not resemble the observed picture presented by observations. A stream wind obtained from a stream function was introduced in place of the geostrophic wind to correct this defect. However, in a diagnostic study, the quasi-geostrophic approximation is acceptable and computational costs are greatly reduced where many data points and data sets are involved. Thus it will be used in this study. (The H subscript on the symbols involving the horizontal wind is dropped in the remainder of the text.)

Lorenz (1955) introduced the concept of available potential energy (APE). He defined it as that energy which would be available for conversion to kinetic energy if the atmosphere were brought hydrostatically to a state of minimum total potential energy through isentropic readjustment. The minimum state is characterized by horizontal stratification of the potential temperature surfaces. An energy flow picture using this definition is displayed as the middle diagram in Fig. 1. The letter "A" represents the portion of the sum of potential and internal energy which can be transformed; G(A) represents the generation of APE; C(A,K) is the conversion of APE to kinetic energy; D(K) denotes the frictional dissipation of kinetic energy. It is clear from this figure that in an hydrostatic, adiabatic, and frictionless atmosphere, the sum of available potential energy and kinetic energy is conserved. A decrease in one must be accompanied by an increase in the other. However APE is exactly zero

when potential temperature surfaces are horizontally stratified. The kinetic energy of the geostrophic wind would likewise be zero in such a case because the pressure surfaces coincide with the potential temperature surfaces. Since the actual wind tends to be largely geostrophic in nature, large values of kinetic energy must therefore correspond to large values of APE. Thus when there is a simultaneous increase of both energy forms, diabatic processes must be responsible. Using Lorenz' (1955) sample calculations, the average amount of total potential energy which is available for conversion to kinetic energy is about one percent. Oort (1964) indicates that the average kinetic energy is smaller than average APE by a factor of three-fourths while Wiin-Nielsen (1967) shows the factor to be one-half. It appears that there is sufficient APE for conversion to kinetic energy.

Wiin-Nielsen (1967, 1968) has pointed out that knowledge of the intensity, i.e., the rate of energy transformation, of the atmospheric general circulation is limited. If thorough measurements of G(A), C(A,K), or D(K) were accessible then this intensity could be ascertained. However the assessment of any of these quantities is not available as a well-known value for the globe or either hemisphere. Generation of APE requires knowledge of the distribution of the diabatic heating and cooling. Conversion of APE to kinetic energy is dependent upon knowing the vertical velocity. Dissipation of kinetic energy is based on frictional effects both in the boundary layer and in the remainder of the atmosphere.

Lacking adequate knowledge about the horizontal components of the frictional force, D(K) could be evaluated as a residual term in the manner of Kung (1966,

1967). Wiin-Nielsen (1968) notes that such a procedure is difficult. He shows that the calculation involves tendencies toward a balance between numerically large quantities. Thus extreme accuracy in the observations of atmospheric data is needed in order to avoid errors. It is doubtful that such accuracy exists even in the dense data collection networks.

The choice of computing either G(A) or C(A,K) is one of selecting equally intricate options. Vertical velocities needed for the conversion term are the result of the divergent part of the horizontal wind. Forecast models employing the quasi-nondivergent and adiabatic assumptions have provided weather predictions for a little over a decade and the results indicate that these approximations yield useful prognoses over short time periods. Based on the resolvable scale of the models this implies that the effects of both the divergent wind and the diabatic processes are small over these short time periods. But if adequate information concerning the diabatic processes were available, then the calculated vertical velocity fields using this knowledge would contain more useful information. This report continues the examination of diabatic processes and the generation of available potential energy.

1.2. PREVIOUS CALCULATIONS

Many calculations for G(A) have used the approximate expression derived by Lorenz (1955). He first shows that the average APE depends on the variance of pressure relative to the isentropic surfaces. This is the result of keeping only the first term of a power series expansion for APE. He then approximates this variance as the variance of temperature on an isobaric level. Using the

isobaric form, G(A) is computed by: (1) determining the deviations from the isobaric area mean for both diabatic processes and temperature, and (2) calculating the volume integral of the covariance of these deviations. Dutton and Johnson (1967), in criticizing the results of investigators who used the simplified expression, argue that the approximation neglects the generation of of APE due to heating (cooling) on an isentropic surface at higher (lower) pres sure. (Isentropic surfaces exhibit strong upward slopes in a poleward direction within the troposphere.) They also mention that the approximation does not retain dependence on total diabatic heating. However, Wiin-Nielsen (1968, Equations 51 and 56) shows that the approximation is energetically consistent with the quasi-geostrophic theory and must be used in studies where the theory is invoked.

Following what has become a common practice, the distribution of any param eter over the globe may be separated into a zonal or mean value and an eddy or remaining value. The eddies constitute the difference after the mean has been subtracted from the total. Oort (1964) compiled the results of many investigators and developed an annual picture of the atmospheric cycle in terms of zonal and eddy quantities. He gives a value of 31×10^{-4} kj m^{-2} sec^{-1} for the generation of zonal APE and -8×10^{-4} kj m^{-2} sec^{-1} for the generation of eddy APE in the space domain. (Values in the space domain are determined by performing calculations on each set of a time series and then averaging the results. Using the terminology of Lorenz (1967), the results in the space domain answer questions concerning the standing zonal and standing eddy circulations. Multiplication by 10^3 converts the units of 10^{-4} kj m^{-2} sec^{-1} to watts m^{-2}.)

Oort's cycle implies that on the average there is heating where it is warm and cooling where it is cold along a longitude circle and just the opposite along a latitude circle. The bottom diagram in Fig. 1 shows the energy flow using the separation of APE and kinetic energy into zonal and eddy components. Directions of the arrows are based on Oort's (1964) results for the space domain.

Smagorinsky, Manabe, and Holloway (1965) reported on the results of a numerical model which did not contain the effects of mountains, land and sea contrast or a hydrological cycle. They obtained a generation of 43×10^{-4} kj m^{-2} sec^{-1} for zonal APE and of -9×10^{-4} kj m^{-2} sec^{-1} for eddy APE. Manabe and Smagorinsky (1967) commented on a model with a hydrological cycle where the lower boundary consists of a wet and flat surface without heat capacity. They computed a generation of 5×10^{-4} kj m^{-2} sec^{-1} for eddy APE apparently due to the large release of latent heat in the tropics.

Dutton and Johnson (1967) applied the expression for the generation of zonal APE in isentropic coordinates to a somewhat arbitrary assignment of the components of Lettau's (1954) heat budget within a two-layer model to compute a generation of 56×10^{-4} kj m^{-2} sec^{-1}. Using the results of Kung's (1966) study of the dissipation of kinetic energy, they concluded that the generation of eddy APE was positive and equal to 8×10^{-4} kj m^{-2} sec^{-1}. Kung (1967) expanded his data to include 1200 GMT observations as well as 0000 GMT soundings over North America. A new computation revised the value of dissipation from 64×10^{-4} kj m^{-2} sec^{-1} downward to 41×10^{-4} kj m^{-2} sec^{-1}. This of course reverses the picture proposed by Dutton and Johnson (1967) since the generation of eddy APE becomes -15×10^{-4} kj m^{-2} sec^{-1} using Kung's newer estimate.

Wiin-Nielsen (1968) has commented on the results of Dutton and Johnson (1967) and Kung (1966, 1967). He points out that the method employed by Dutton and Johnson applies to the mixed space-time domain while Kung's results refer to the space domain. (The mixed domain gives results which apply to the sum of the time-mean and standing zonal motions and the sum of the transient and standing eddy circulations.) Oort (1964) displays the dangers involved in mixing such computations in that the generation of eddy APE has opposite signs in the two regimes. Wiin-Nielsen (1968) also mentions the limitations involved in using cross-sectional data along a particular meridian to create zonal averages.

Lawniczak (1969), using a 4-layer quasi-nondivergent model, calculated a value for the generation of zonal APE of 45×10^{-4} kj m^{-2} sec^{-1} and a value of -22×10^{-4} kj m^{-2} sec^{-1} for the generation of eddy APE based on March 1963 data. These values were computed in a volume bounded by the pressure levels at 100 and 30 cb and the latitude rings at 28.75N and 88.75N.

1.3. THE PURPOSE OF THIS STUDY

Results of most of the previous investigations of diabatic processes and the generation of APE, other than numerical simulation, are based on models with limited vertical resolution. These models use observational or climatological data and examples are Wiin-Nielsen and Brown (1960), Brown (1964), and Dutton and Johnson (1967). These investigations must confront the problems associated with sparse data coverage and analysis errors. Although the numerical simulation models do not suffer these defects they do impose certain artificialities due to imperfect knowledge of the real behavior of the atmosphere. To date they have not included a realistic treatment of the lower boundary effects.

The present observational system of upper-air soundings of heights and winds which assumes the hydrostatic balance will remain the primary source of atmospheric data for some time to come. Application of the simple quasi-geostrophic theory seems reasonable in light of the amount and geographic distribution of data.

The purpose of this inquiry is to apply the model described by Lawniczak (1969) to a data set covering more of the surface area of the Northern Hemisphere using a 5-layer version of the model Chapter 2 contains the development of the equations used to calculate diabatic heating and cooling and the zonal and eddy components of G(A). The data and the application of the equations also are discussed in Chapter 2. Results of the computations are presented in Chapter 3 and the conclusions and a summary are provided in Chapter 4. The Appendix contains the finite difference forms for the equations used in the various calculations.

CHAPTER 2

THE EQUATIONS AND THE DATA

2.1. THE BASIC EQUATION FOR DIABATIC PROCESSES

Wiin-Nielsen and Brown (1960) used a two-level, quasi-nondivergent model to calculate diabatic heating and cooling from observational data. Using the same model, Brown (1964) extended the study to a larger data sample and introduced a more reasonable lower boundary condition involving the terrain and frictionally induced vertical velocities. However, frictional forces were neglected in the vorticity equation and as in the previous investigation static stability was made a constant for the layer 80-40 cb. Lawniczak (1969) applied a 7-layer quasi-nondivergent model to the National Meteorological Center's (NMC) analyses for March 1963, in which these frictional effects were included and static stability was allowed to be pressure dependent. However, the results of the diabatic computations above 30 cb were unusable because of the failure of the quasi-nondivergent theory there. The theory fails because (1) of the existence of a maximum wind layer which leads to a significant imbalance between the local time change and the horizontal advection terms involving geostrophic potential vorticity, and (2) static stability values increase by at least one order of magnitude there. Diabatic calculations south of 30N were incorrect because of boundary errors associated with the NMC analyses. This report is a continuation of these investigations with the added refinements of a data set which covers the Northern Hemisphere and an appropriate modeling of static stability for the tropospheric layer from 100 to 30 cb.

The vorticity and thermodynamic equations for a quasi-geostrophic model

including the effects of diabatic processes and friction have the form

$$\frac{\partial \zeta}{\partial t} + \vec{V}\cdot\nabla(\zeta+f) = \bar{f}\frac{\partial \omega}{\partial p} + \left(\frac{\partial F_y}{\partial x} - \frac{\partial F_x}{\partial y}\right) \tag{2.1}$$

and

$$\frac{\partial}{\partial t}\left(\frac{\partial \Phi}{\partial p}\right) + \vec{V}\cdot\nabla\left(\frac{\partial \Phi}{\partial p}\right) + \sigma\omega = -\frac{RH}{c_p p} \tag{2.2}$$

respectively.

In the above equations, $\vec{V}$ is the horizontal geostrophic wind which is computed from $\vec{V} = \vec{k} \times \frac{g}{f}\nabla z$ where $\vec{k}$ is the vertically-directed unit vector, $g = 9.8$ m sec^{-2} is the acceleration of gravity, f is the Coriolis parameter where $\bar{f}$ is its value at 45N, z is the height above mean sea level, and $\nabla = \frac{\partial}{\partial x}\vec{i} + \frac{\partial}{\partial y}\vec{j}$ is the horizontal part of the gradient operator where $\vec{i}$ and $\vec{j}$ are unit vectors; $\zeta = \frac{\partial v}{\partial x} - \frac{\partial u}{\partial y}$ is the relative vorticity; ω is the vertical p-velocity, $\frac{dp}{dt}$, where p is pressure and t is time; $\Phi = gz$; $\sigma = -\alpha\frac{\partial(\ell n\theta)}{\partial p}$ is the static stability where α is the specific volume and θ is the potential temperature; $R = 287$ kj ton^{-1} deg^{-1} is the gas constant for air; $c_p = 1004$ kj ton^{-1} deg^{-1} is the specific heat at constant pressure; H is the time rate of diabatic heating or cooling per unit mass where a positive quantity means heating; F_x and F_y are the x and y components of the frictional force respectively.

In (2.1) the vertical advection of vorticity and the terms expressing the turning of the vortex tubes have been neglected. This is equivalent to neglecting the vertical advection of momentum in the first two equations of motion from which (2.1) is derived. In the first term on the right side of (2.1), $\bar{f}$ replaces $(f+\zeta)$. Wiin-Nielsen (1959) has shown that these deletions and approximations are required in the simplified vorticity equation in order

to satisfy and be consistent with certain properties which the complete vorticity equation exhibits.

Solving (2.2) for ω gives the result

$$\omega = -\left[\frac{\partial}{\partial t}\left(\frac{1}{\sigma}\frac{\partial\Phi}{\partial p}\right) + \vec{V}\cdot\nabla\left(\frac{1}{\sigma}\frac{\partial\Phi}{\partial p}\right) + \frac{RH}{c_p\sigma p}\right] . \tag{2.3}$$

If (2.3) is differentiated with respect to pressure, the equation

$$\frac{\partial\omega}{\partial p} = -\left[\frac{\partial}{\partial t}\frac{\partial}{\partial p}\left(\frac{1}{\sigma}\frac{\partial\Phi}{\partial p}\right) + \vec{V}\cdot\nabla\frac{\partial}{\partial p}\left(\frac{1}{\sigma}\frac{\partial\Phi}{\partial p}\right) + \frac{R}{c_p}\frac{\partial}{\partial p}\left(\frac{H}{\sigma p}\right)\right] \tag{2.4}$$

is obtained. Substituting (2.4) into (2.1) produces

$$\frac{\partial\zeta}{\partial t} + \vec{V}\cdot\nabla(\zeta+f) + \frac{\partial}{\partial t}\frac{\partial}{\partial p}\left(\frac{\bar{f}}{\sigma}\frac{\partial\Phi}{\partial p}\right) + \vec{V}\cdot\nabla\frac{\partial}{\partial p}\left(\frac{\bar{f}}{\sigma}\frac{\partial\Phi}{\partial p}\right) = -\frac{\bar{f}R}{c_p}\frac{\partial}{\partial p}\left(\frac{H}{\sigma p}\right) + \left(\frac{\partial F_y}{\partial x} - \frac{\partial F_x}{\partial y}\right) . \tag{2.5}$$

Letting

$$\xi = \zeta + f + \frac{\partial}{\partial p}\left(\frac{\bar{f}}{\sigma}\frac{\partial\Phi}{\partial p}\right) , \tag{2.6}$$

represent the geostrophic potential vorticity, (2.5) can be rewritten as

$$\frac{\partial}{\partial p}\left(\frac{H}{\sigma p}\right) = -\frac{c_p}{\bar{f}R}\left[\frac{\partial\xi}{\partial t} + \vec{V}\cdot\nabla\xi - \left(\frac{\partial F_y}{\partial x} - \frac{\partial F_x}{\partial y}\right)\right] . \tag{2.7}$$

Integrating (2.7) with respect to pressure from $p = p_o$, where the subscript o indicates a lower boundary value, to some arbitrary pressure $p = p$, gives the basic equation for calculating diabatic processes,

$$\boxed{H = \frac{\sigma p}{\sigma_o p_o} H_o + \sigma p \int_{p=p_o}^{p=p} -\frac{c_p}{\bar{f}R}\left[\frac{\partial\xi}{\partial t} + \vec{V}\cdot\nabla\xi - \left(\frac{\partial F_y}{\partial x} - \frac{\partial F_x}{\partial y}\right)\right] dp} . \tag{2.8}$$

The terms inside the brackets can be computed from observations on pressure levels. Thus the diabatic heating and cooling at any level can be calculated provided that H_o can be determined.

2.2. CALCULATION OF FRICTIONAL EFFECTS

Phillips (1963) explained that a necessary condition for geostrophic balance to be assumed is that frictional forces are small compared to the Coriolis acceleration. This assumption means that important frictional effects must be limited to the boundary layer. For convenience it will be assumed that the effective lower boundary of the atmosphere is 92.5 cb. Assuming also that the depth of the layer in which the frictional forces vanish at the top is 15 cb, then the 85-cb level is the middle of this layer. The effects of the frictional forces in the boundary layer are assigned to the 85-cb level calculations.

Let

$$F_x = g \frac{\partial \tau_x}{\partial p} \tag{2.9}$$

and

$$F_y = g \frac{\partial \tau_y}{\partial p} \tag{2.10}$$

where τ_x and τ_y are the surface stress components. Substituting (2.9) and (2.10) into the term representing the frictional effects in (2.8) leads to

$$\left(\frac{\partial F_y}{\partial x} - \frac{\partial F_x}{\partial y} \right) = g \frac{\partial}{\partial p} \left(\frac{\partial \tau_y}{\partial x} - \frac{\partial \tau_x}{\partial y} \right) . \tag{2.11}$$

Since the stress vanishes at the top of the friction layer by assumption, using finite differencing (2.11) becomes

$$g\frac{\partial}{\partial p}\left(\frac{\partial \tau_y}{\partial x}-\frac{\partial \tau_x}{\partial y}\right)=\frac{g}{\Delta p}\left(\frac{\partial \tau_y}{\partial x}-\frac{\partial \tau_x}{\partial y}\right)_o \tag{2.12}$$

where $\Delta p = 15$ cb.

If the terrain stress is further assumed to be proportional to the square of the surface geostrophic wind in the manner of Lettau (1959) and Cressman (1960), these stress components can be approximated as

$$\tau_x = C_D \rho_o u_o V_o , \quad \tau_y = C_D \rho_o v_o V_o . \tag{2.13}$$

Using (2.13), (2.12) can be written as

$$\frac{g}{\Delta p}\left(\frac{\partial \tau_y}{\partial x}-\frac{\partial \tau_x}{\partial y}\right)_o = \frac{g p_o}{\Delta p R T_o}\left[\frac{\partial}{\partial x}\left(C_D v_o V_o\right)-\frac{\partial}{\partial y}\left(C_D u_o V_o\right)\right] . \tag{2.14}$$

The equation of state, $p = \rho RT$, has been used in (2.14) to eliminate density which was itself assumed to be constant with respect to local space differentiation. In (2.14), p_o is the pressure at the terrain height; C_D is the coefficient of drag based on Cressman's (1960) work; V_o is the resultant geostrophic surface wind and u_o and v_o are its components; T_o is the temperature at terrain height. The computation of pressure, temperature, and geostrophic surface wind at the lower boundary is performed using techniques developed by Clarke and Lawniczak (1962) which utilize the terrain data of Berkofsky and Bertoni (1955). The procedure is outlined in the Appendix.

In (2.14) a further assumption is made that the local space variations of $C_D V_o$ are negligible. The final form for calculating friction is therefore

$$\frac{g}{\Delta p}\left(\frac{\partial \tau_y}{\partial x}-\frac{\partial \tau_x}{\partial y}\right)_o = \frac{g p_o C_D V_o \zeta_o}{\Delta p R T_o} \tag{2.15}$$

where ζ_o is the surface relative vorticity.

2.3. DIABATIC PROCESSES AT THE LOWER BOUNDARY

Applying the hydrostatic equation, $\frac{\partial \Phi}{\partial p} = -\alpha$, and the state equation to (2.2) yields

$$\frac{\partial T_o}{\partial t} + \vec{V}_o \cdot \nabla T_o - \frac{p_o \sigma_o \omega_{\ell o}}{R} = \frac{H_o}{c_p} \tag{2.16}$$

or

$$\boxed{H_o = c_p \left(\frac{\partial T_o}{\partial t} + \vec{V}_o \cdot \nabla T_o \right) - \frac{c_p}{R} p_o \sigma_o \omega_{\ell o}} \tag{2.17}$$

where σ_o is the static stability at the terrain height and $\omega_{\ell o}$ is the vertical velocity in the lower boundary. Within quasi-geostrophic theory static stability can be at most a function of pressure. Based on Gates' (1960) and Lawniczak's (1969) computations for the troposphere, it is modeled with the form

$$\sigma = \frac{\bar{\sigma} \bar{p}}{p} \tag{2.18}$$

where $\bar{\sigma} = 1\ m^2\ sec^{-2}\ cb^{-2}$ and $\bar{p} = 100$ cb.

The omega in the lower boundary, $\omega_{\ell o}$, is calculated following the results of Cressman (1960) and Haltiner, Clarke, and Lawniczak (1963). Their results show that the vertical velocity induced by the terrain can be approximated as

$$\omega_o = \vec{V}_o \cdot \nabla p_o \tag{2.19}$$

and the frictionally induced omega can be computed from

$$\omega_{\ell f} = - \frac{g p_o C_D V_o \zeta_o}{f R T_o} \tag{2.20}$$

where ω_o is the terrain vertical velocity and $\omega_{\ell f}$ is the friction vertical velocity. Therefore

$$\omega_{\ell o} = \omega_o + \omega_{\ell f} \quad . \tag{2.21}$$

The integrand of (2.8) can be computed at the pressure levels for which data are available. Letting B equal the integrand and using the results of (2.17), the diabatic processes can be calculated at the required levels by using the following summation:

$$\boxed{H_p = H_o + 100 \left[- \sum_{i=1}^{i=ip} B_i (\Delta p)_i \right]} \tag{2.22}$$

where H_p is the result at the top of the ip-th layer.

2.4. THE GENERATION OF AVAILABLE POTENTIAL ENERGY

It has been shown by Lorenz (1955) that the computation of the generation of APE, using pressure as the vertical coordinate, depends on the covariance of the deviations of temperature and diabatic processes from their areal averages. As shown by Wiin-Nielsen and Brown (1960), this generation or rate of energy conversion can be calculated from

$$G = - \frac{R}{c_p} \int_{p=o}^{p=p_o} \frac{1}{\sigma p} \int_S H' \left(\frac{\partial \Phi}{\partial p} \right)' \, dS dp \tag{2.23}$$

where G represents the generation of APE in the units kj sec^{-1}; S is the surface area and $dS = a^2 \cos\varphi \, d\lambda \, d\varphi$ where a is the radius of the earth, φ is the latitude, and $d\lambda$ and $d\varphi$ are the increments of latitude and longitude respectively;

the prime indicates that the value is the deviation from the area mean value. The area mean value is calculated from

$$(\overline{\ }) = \frac{a^2}{S} \int_{\varphi_1}^{\varphi_2} \int_{o}^{2\pi} (\ ) \cos\varphi d\lambda d\varphi \tag{2.24}$$

where the over-bar denotes the average of the parameter; $S = 2\pi a^2(\sin \varphi_2 - \sin \varphi_1)$ is the area of the region and φ_1 and φ_2 are the limiting latitudes.

Using techniques similar to those employed by Wiin-Nielsen, Brown, and Drake (1963), the generation term can be separated into wave-number domain such that

$$G = G_z + G_e \tag{2.25}$$

where G_z measures the contribution from the zonal or the north-south covariance and G_e measures the eddy portion or the east-west covariance. Letting the Fourier series

$$H' = Y_o(\varphi) + \sum_{n=1}^{\infty} [Y_n(\varphi) \cos n\lambda + Z_n(\varphi) \sin n\lambda] \tag{2.26}$$

represent the diabatic deviation field and

$$\left(\frac{\partial \Phi}{\partial p}\right)' = y_o(\varphi) + \sum_{n=1}^{\infty} [y_n(\varphi) \cos n\lambda + z_n(\varphi) \sin n\lambda] \tag{2.27}$$

represent the thickness deviation field, the contribution from the north-south covariance becomes

$$G_z = -\frac{2\pi R a^2}{c_p} \int_{p=o}^{p=p_o} \frac{1}{\sigma p} \int_{\varphi_1}^{\varphi_2} Y_o y_o \cos\varphi d\varphi dp \ . \tag{2.28}$$

The calculation of the generation due to the eddies can be expressed as

$$G_e = -\frac{\pi Ra^2}{c_p}\int_{p=o}^{p=p_o}\frac{1}{\sigma p}\int_{\varphi_1}^{\varphi_2}\sum_{n=1}^{N}[Y_n y_n + Z_n z_n]\cos\varphi d\varphi dp \quad . \tag{2.29}$$

Using numerical approximation, (2.28) and (2.29) become

$$\boxed{G_z = -\frac{\pi Ra^2\Delta\varphi}{50\cdot c_p}\sum_{i=1}^{i=m}\Delta p_i \sum_{j=1}^{j=k} Y_o y_o \cos\varphi_j} \tag{2.30}$$

and

$$\boxed{G_e = -\frac{\pi Ra^2\Delta\varphi}{100\cdot c_p}\sum_{i=1}^{i=m}\Delta p_i \sum_{j=1}^{j=k}\sum_{n=1}^{N}[Y_n y_n + Z_n z_n]\cos\varphi_j} \tag{2.31}$$

where m determines the vertical resolution; k determines the latitudinal resolution; N is the numerical limit on the harmonic components; and $\Delta\varphi$ is the latitude increment. Note that for a particular n, (2.31) becomes

$$G_{e,n} = -\frac{\pi Ra^2\Delta\varphi}{100\cdot c_p}\sum_{i=1}^{i=m}\Delta p_i \sum_{j=1}^{j=k}[Y_n y_n + Z_n z_n]\cos\varphi_j \quad . \tag{2.32}$$

Dividing (2.30) and (2.31) by S will give the generation in units of kj m^{-2} sec^{-1}.

2.5. INPUT DATA

Data used in this investigation are the Fleet Numerical Weather Central (FNWC), Monterey, California, routine objective height analyses of January 1969. They consist of geopotential fields for 0000 GMT and 1200 GMT at 100,

85, 70, 50, 40, and 30 cb and are complete, i.e., there are no missing analyses, as well as vertically consistent, i.e., statically stable from one layer to the next.

The analyses consist of grid-point values at 3969 points for each level on the FNWC array. This array, which contains the equator as an inscribed circle, uses a polar stereographic projection true at 60N where the distance between grid points is 381 km at this latitude. Figures 2 and 3 are examples of typical surface data and 50-cb radiometersonde data coverage, respectively. The numerals indicate the number of reports which influenced that particular grid point during the analysis cycle. The numeral "9" means nine or more reports were involved.

The analysis model employed by FNWC is described by Holl, Bibbo, and Clark (1963). Briefly, in the model, temperature is linear in pressure to the R/c_p power and static stability is computed using

$$\sigma^* = -Rp_o^{-R/c_p} p^{1+R/c_p} \frac{d\theta}{dp} \qquad (2.33)$$

where σ^* has units of velocity squared and is equal to σp^2. The model partitions the column from 100 to 20 cb into five layers. A one-to-one transform is developed between the heights of 7 mandatory pressure levels and the 100-cb height, the thickness for the layer from 100 to 50 cb and five static stability parameters. An inverse transform is available so that given one set, the other can be generated. Within the model, the acceptable reports of heights at 100 and 50 cb are unaltered. The 100-cb analysis is closely related to the surface analysis where the amount of data exceeds the available upper-air soundings by a factor of 8. Above 50 cb, there is less data generally available and the

Fig. 2. Typical surface data coverage.

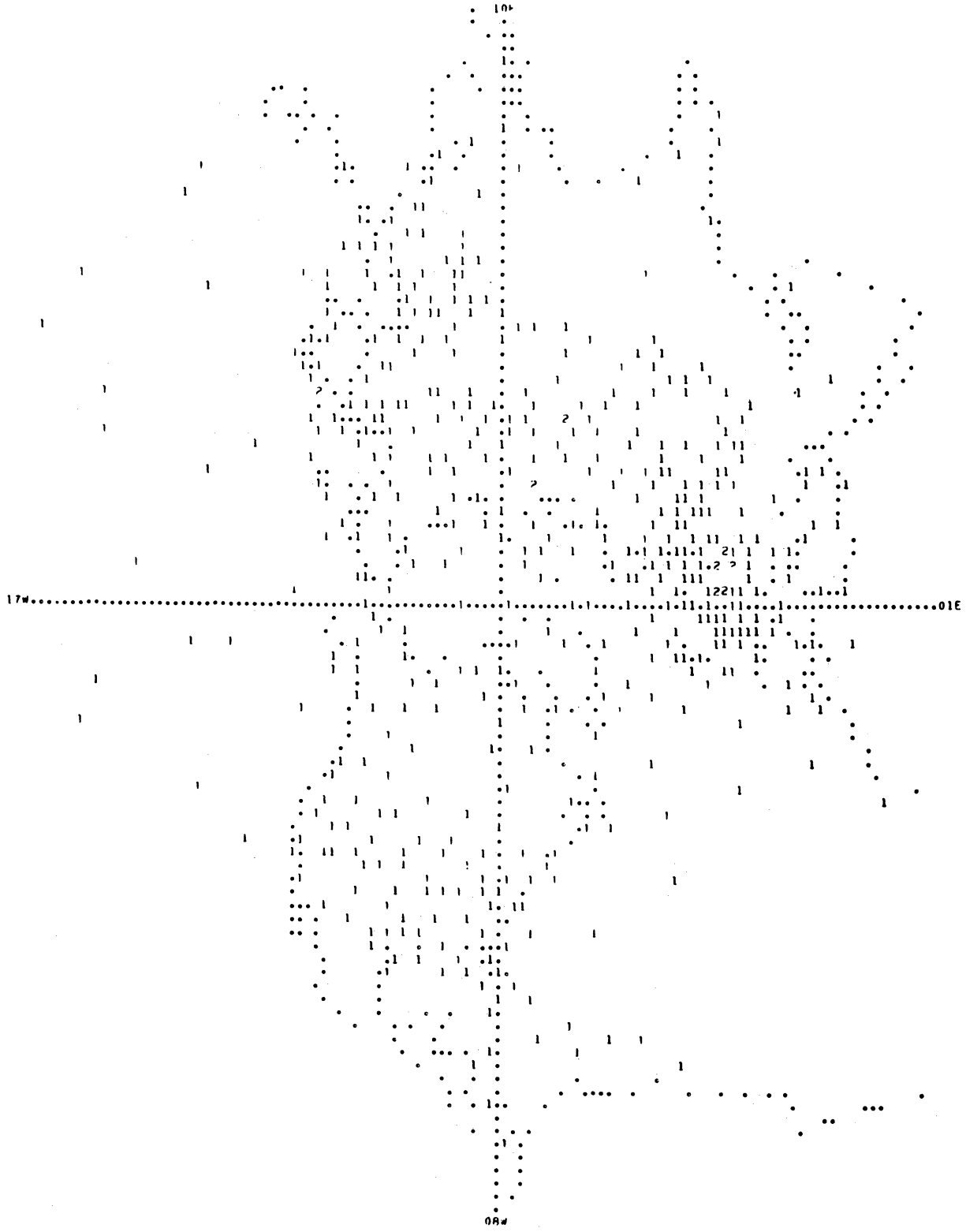

Fig. 3. Typical 50-cb radiometersonde data coverage.

inaccuracies are larger. Also a short-range forecast which has received special emphasis is used as the first approximation for the 50-cb level. The surface analysis and the 50-cb forecast are used to eliminate erroneous data at those levels. After correcting the static stability values of the soundings, (which usually involves correcting negative values although there are instances where values are too large), the seven parameters are analyzed and the resultant analyses are inverted to produce the desired geopotential fields. The corrections in static stability generally involve height changes of less than 10 meters from the reported values at levels other than 100 and 50 cb. (At this writing, FNWC has shifted to a 10-layer version of this model which extends from 100 to 10 cb.)

2.6. COMPUTATIONS OF H_p, B, H_o, AND G(A)

Figure 4 shows the levels at which H_p and B can be calculated based on the available data. For convenience the lower boundary effects, represented by the diabatic term, H_o, have been assigned to the 92.5-cb level. The effects of the frictional forces are included in the calculation of B at the 85-cb level. Once H_p fields have been computed, the generation of APE can be determined. Based on the available data, the vertical resolution parameter, m, in (2.30) and (2.31), takes on the value 5. The latitude increment is taken as 2.5 deg and the region is set as that bounded by the latitude rings at 5N and 87.5N. Thus Φ_1 = 3.75N and Φ_2 = 88.75N while k takes on the value 34. An artificial "wall" is introduced in the diabatic computations in that the values of the sine and Coriolis parameters at 4N are assigned to all grid points south of that latitude.

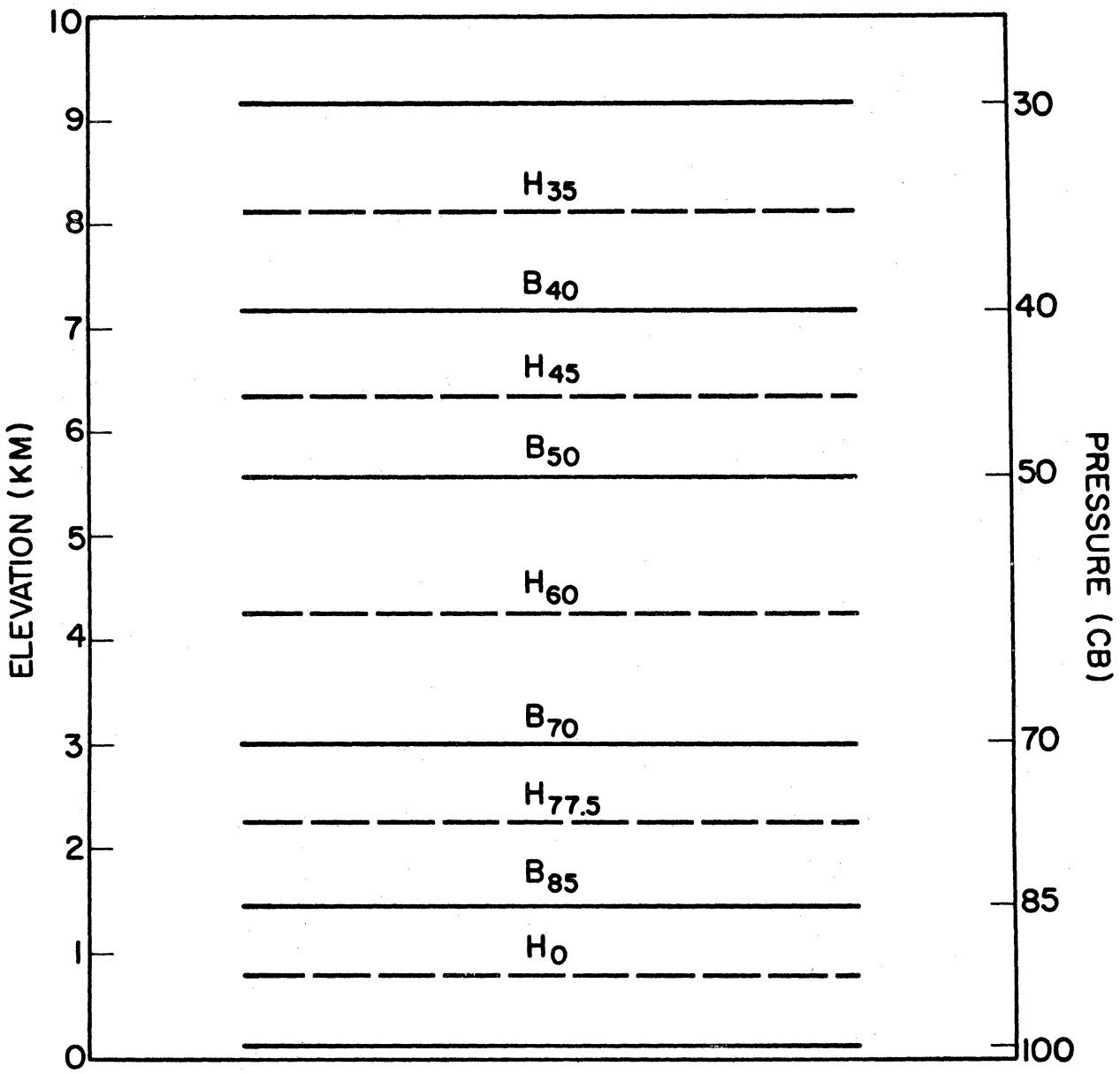

Fig. 4. The levels at which the integrand of (2.8), B, and the diabatic processes, H, are calculated.

CHAPTER 3

RESULTS OF THE COMPUTATIONS

3.1. MEAN DIABATIC PROCESSES FOR JANUARY 1969

Calculations of H and B were made using the data as illustrated in Fig. 4. Computations were made using the finite difference equations given in the Appendix and the results are available at twelve-hourly intervals for the month. Figure 5 depicts the zonally averaged values of the diabatic processes for January 1969. The units are 10^{-2} k.j sec^{-1} ton^{-1} and multiplication by 0.864 converts them to deg day^{-1}.

The most pronounced feature in Fig. 5 is the vertical orientation of the patterns. The values and the gradient south of about 12N, although correct in sign, suggest that the results are unreliable. This is really no surprise since the quasi-geostrophic model cannot be expected to produce acceptable results in low latitudes where the sine has such small values.

The vertical nature of the zero line near 50N is similar to that shown by Lawniczak (1969) for March 1963. Snow-cover probability charts prepared by Dickson and Posey (1967) suggest that the existence of snow or ice cover at the surface is responsible. Sellers (1965) shows that between 50N and 70N, oceans cover about 36% of the surface area. In January, most of the area north of 70N can be considered to be covered by either ice or snow. Since the January coverage charts show that the probability line representing the value 1 extends to about 50N on the average throughout the continental areas of the Hemisphere, it appears that this surface feature is significant in effecting a separation between the areas of mean heating and cooling throughout the troposphere. Note

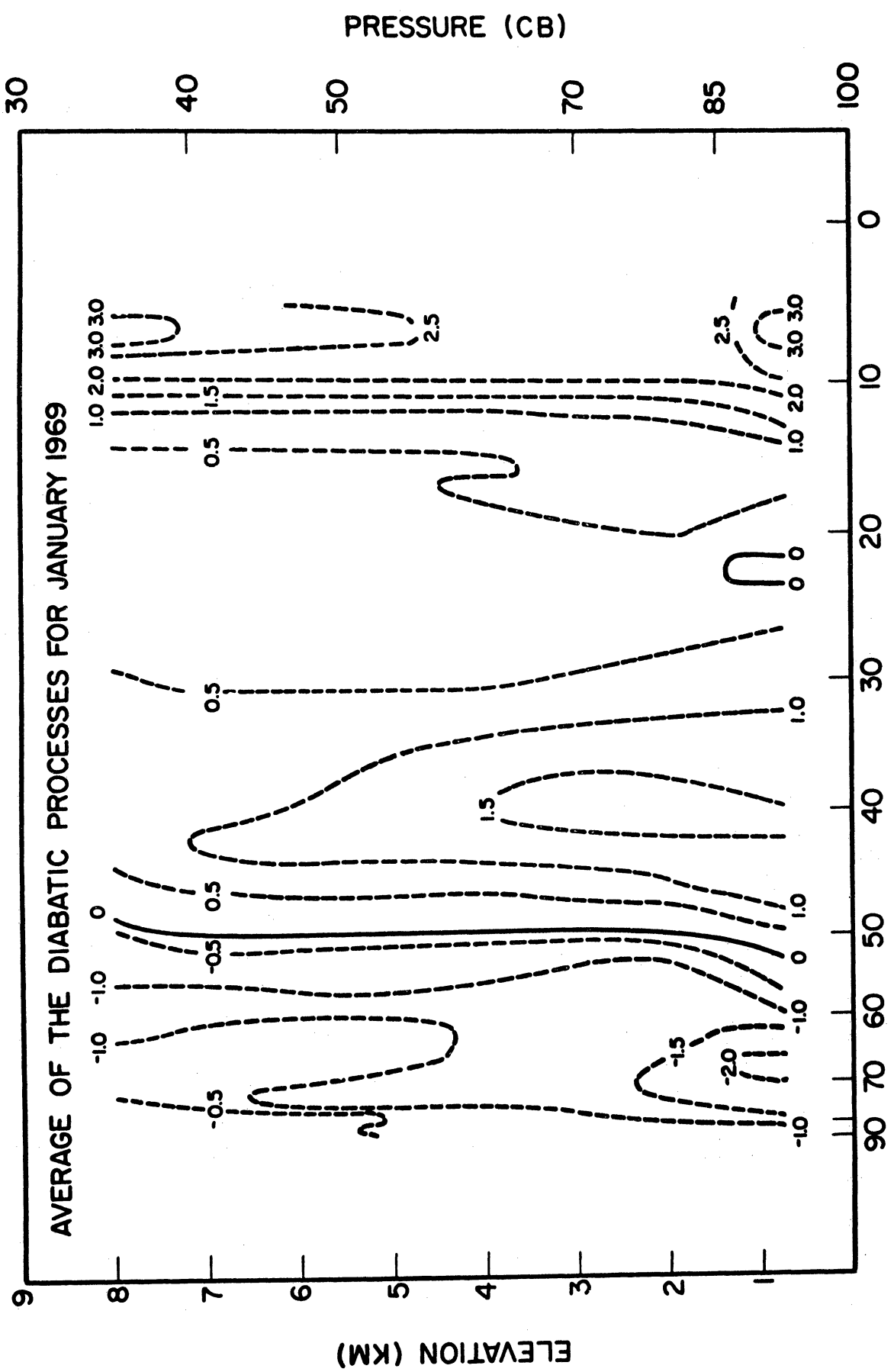

Fig. 5. Zonal average of the diabatic processes for January 1969, as a function of the sine of the latitude and pressure in the units of 10^{-2} kj sec^{-1} ton^{-1}.

that maximum cooling occurs between 65N and 70N near the surface and maximum heating, excluding the results near and south of 10N which are suspect, occurs around 40N, also in the lowest layers.

Figure 6 is the result of plotting the vertically integrated mean values of the information displayed in Fig. 5. Again neglecting the lowest latitudes, maximum heating (cooling) occurs near 42N (65N). These features compare favorably with the mean winter calculations presented by Palmen and Newton (1969). (For a 70-cb layer, 1 ly min^{-1} is equal to 9.765×10^{-2} kj sec^{-1} ton^{-1}.) Although their computations show a maximum (minimum) between the equator and 10N (70N and 90N), they point out that the magnitude of the values for sensible heat transfer in these bands (computed as a residual) makes the magnitude of these particular features unlikely.

However, they do indicate that net cooling takes place during winter in the band between 10N and 30N. This of course is in contrast to the results shown in Fig. 6. Perhaps this difference could be explained on the basis that only the mean values for one month are displayed in Fig. 6. At least on additional aspect can be examined however.

Under quasi-geostrophic assumptions, if an area average of (2.2) is taken over the globe, only the mean values of the first and last term remain. Now even only for one month, the first term will have a very small value which means that the mean heating likewise must be very small. Assuming that the contributions from the horizontal and vertical advective terms remain negligible when averaging is taken over a portion of the globe, then the value for area mean heating for that portion should remain small. Regardless, subtracting the area mean value would seemingly adjust the computed values in the proper direction.

The area mean of the results given by Palmen and Newton (1969), ignoring the bands from the equator to 10N and from 70N to 90N, for mean winter conditions is -0.35×10^{-2} kj sec^{-1} ton^{-1}. Correcting with this result, the maximum

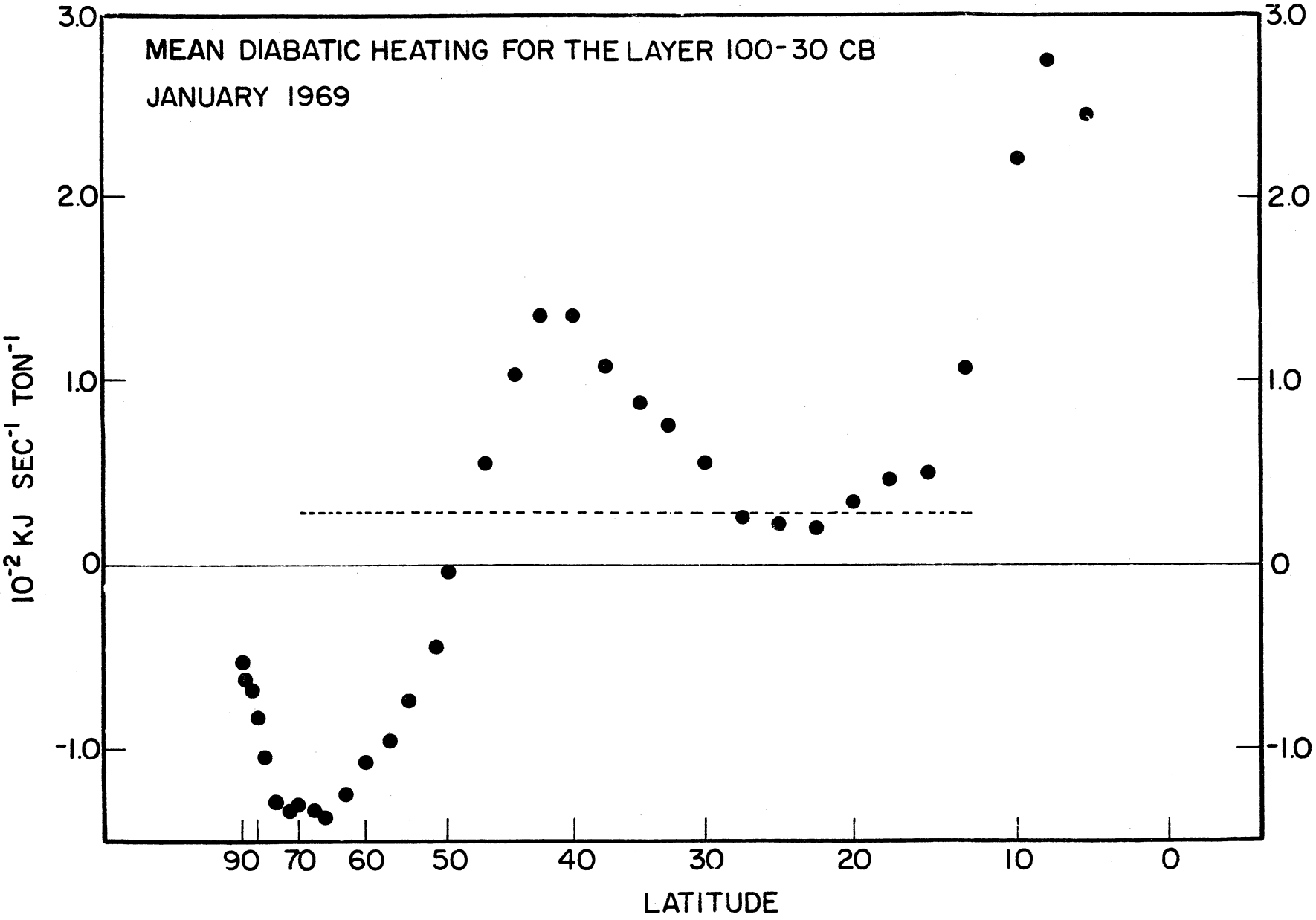

Fig. 6. Mean diabatic processes in the layer from 100 to 30 cb for January 1969. Abscissa is sine of the latitude.

heating (cooling) based on their results is 0.74×10^{-2} kj sec^{-1} ton^{-1} (0.83×10^{-2} kj sec^{-1} ton^{-1}) near 35N (65N). Likewise, the area mean heating based on the results in Fig. 6 for that portion from 11.25N to 71.25N is 0.28×10^{-2} kj sec^{-1} ton^{-1}. The dashed line in Fig. 6 represents the corrected position of the origin using this result. (Based on the results of the calculations in the bands from 12.5N to 87.5N, the area mean value is 0.19×10^{-2} kj sec^{-1} ton^{-1}.) Thus, based on these corrected results for January 1969, the maximum heating (cooling) is 1.07×10^{-2} kj sec^{-1} ton^{-1} (1.65×10^{-2} kj sec^{-1} ton^{-1}) near 42N (65N). As can be seen, with the adjustment, net cooling is indicated in the bands between 20N and 30N.

The main features of Fig. 6 can be given physical interpretation. Cooling effects due to strong long-wave radiation and the underlying snow and ice cover, and small latent heat release contribute to the intense polar minimum. Polar front activity, with the associated large contributions from latent heat release and sensible heat transfer, is responsible for the mid-latitude maximum. The downward branch of the Hadley circulation that suppresses cloudiness and latent heat release is largely responsible for the sub-tropical secondary minimum. Whether or not net heating or cooling is the result is not clear and further computations are required.

Using the results of Fig. 6, 48.75N was used to separate the mean heating and cooling regions. Figure 7 contains the area mean values within each layer for these two regions. (At this point, a decision was made to limit all subsequent computations to the volume between 11.25N and 88.75N.) In still another way, this figure again shows that maxima in heating and cooling occur in the lower troposphere.

3.2. MEAN DIABATIC EFFECTS FOR THE VARIOUS LEVELS

Within the troposphere the important diabatic processes are the absorption of solar radiation, the emission of long wave radiation, the release of latent

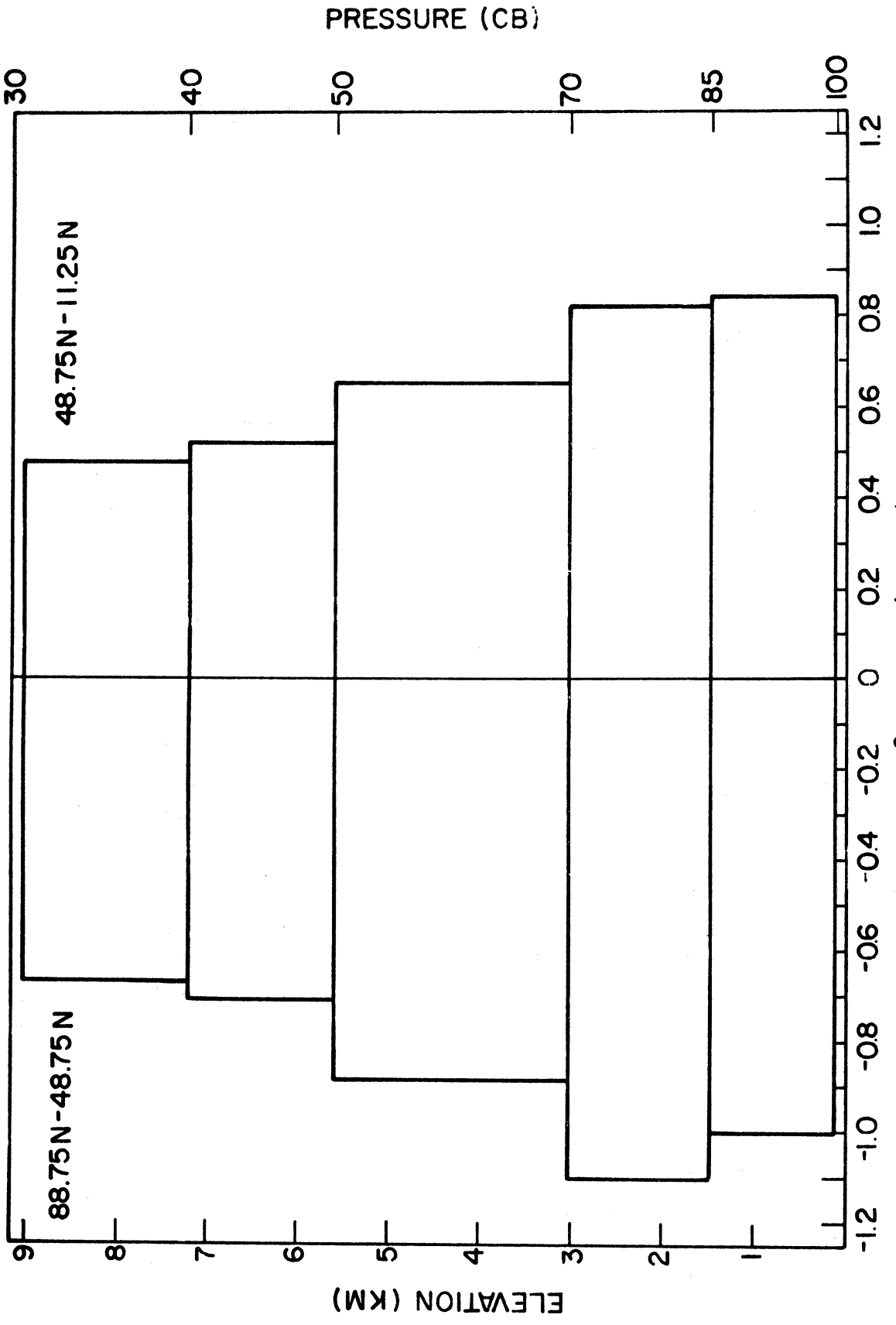

Fig. 7. Area mean values for the diabatic processes within the indicated layers for the heating and cooling regions for January 1969.

heat (provided that some condensate returns to the surface as precipitation), and the transfer of sensible heat across the earth-atmosphere interface. The method of computing the diabatic effects used here precludes the separation into contributions from the components. Some qualitative remarks can be made however.

Within the total depth of the atmosphere the cooling effect of the divergence of long wave radiation flux is the dominant element. In the middle latitudes and the tropics, the contributions from the net gain of latent heat release, solar absorption and the boundary flux are important in the lower troposphere, i.e., the layer from 100 to 50 cb. Cooling effects of long wave radiation should dominate the layer above 50 cb in the high troposphere, low stratosphere, and the polar troposphere.

Monthly averages of the diabatic processes due to the presence of a lower boundary are displayed in Fig. 8. (Areas where average heating occurred during the month are cross-hatched and representative values for maximum rates of heating and cooling are plotted in the appropriate regions.) Phillips (1963) has shown that a maximum heating rate consistent with the geostrophic assumption is of the order 0.1 kj sec^{-1} ton^{-1}. For the calculation of the lower boundary diabatic processes, a limit was set on the magnitude of this computation of 0.7 kj sec^{-1} ton^{-1}. Of the 3969 grid points, an average of 250 points failed this limit and were reset to the limit. A sample evaluation indicates that probably an average of less than 4 points were reset in the region north of 10N.

Patterns presented in Fig. 8 are based on calculations using (2.17). They are therefore the results of the averages of the local time change in and the horizontal advection of the temperature at terrain height and the vertical velocities induced by the surface. (The Appendix contains Fig. 22 which shows the mean terrain-height temperature for January 1969.) Effects of heat transport across the interface are probably wholly contained in this computation.

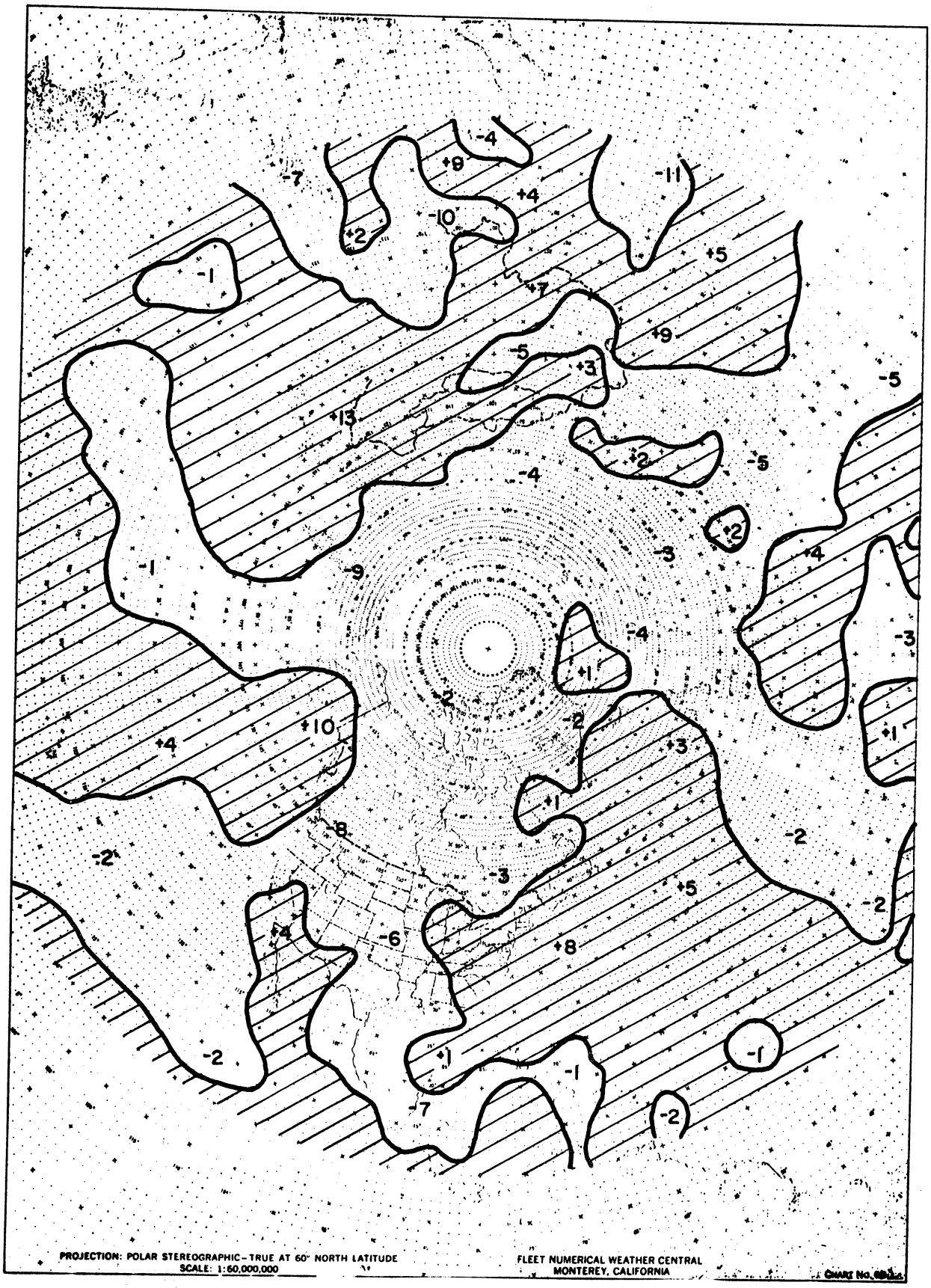

Fig. 8. Monthly average of the diabatic processes at the lower boundary for January 1969, in the units 10^{-2} kj sec^{-1} ton^{-1}.

In general, the patterns in Fig. 8 show the influence of continental cooling and oceanic warming on the lower boundary effects. But the fact that this average has a variable pressure base should not be forgotten. As can be seen in Fig. 21 in the Appendix, this base ranges from pressure greater than 100 cb to pressure lower than 60 cb. Thus there are regions in which latent heat release and warming due to radiational trapping by low clouds are strong modifying influences in the lower boundary.

Figure 8 indicates that maximum heating took place in the Sea of Japan and the Gulf of Alaska while maximum cooling occurred neat Madras, India, and in the Gulf of Tonkin. The tongue of relatively weak cooling in the mid-Pacific Ocean is most likely related to a mean polar front position for the month.

Figures 9 and 10 show the average diabatic pattern for the 77.5- and 60-cb level, respectively. Figure 11 contains the mean 70-cb height contours taken from the April 1969, issue of the Monthly Weather Review. Strong blocks at high latitudes along 40W and 160W, and an intense circulation pattern centered in the Sea of Okhotsk are the dominant features depicted in Fig. 11. The patterns at 77.5 and 60 cb are essentially the same as for the lower boundary. However the shift toward smaller scale features, particularly noticeable by 60 cb, suggest that the complex contributions by long wave radiation trapping and the release of latent heat have become important.

The outstanding features of these patterns are the heating regions associated with the Alaskan and Greenland blocks, and the Atlantic and Pacific Oceans. Cooling areas associated with the central United States are noteworthy. Wagner (1969) reports that the western and northern sections of the United States along with much of the Mississippi Valley and Florida received more than

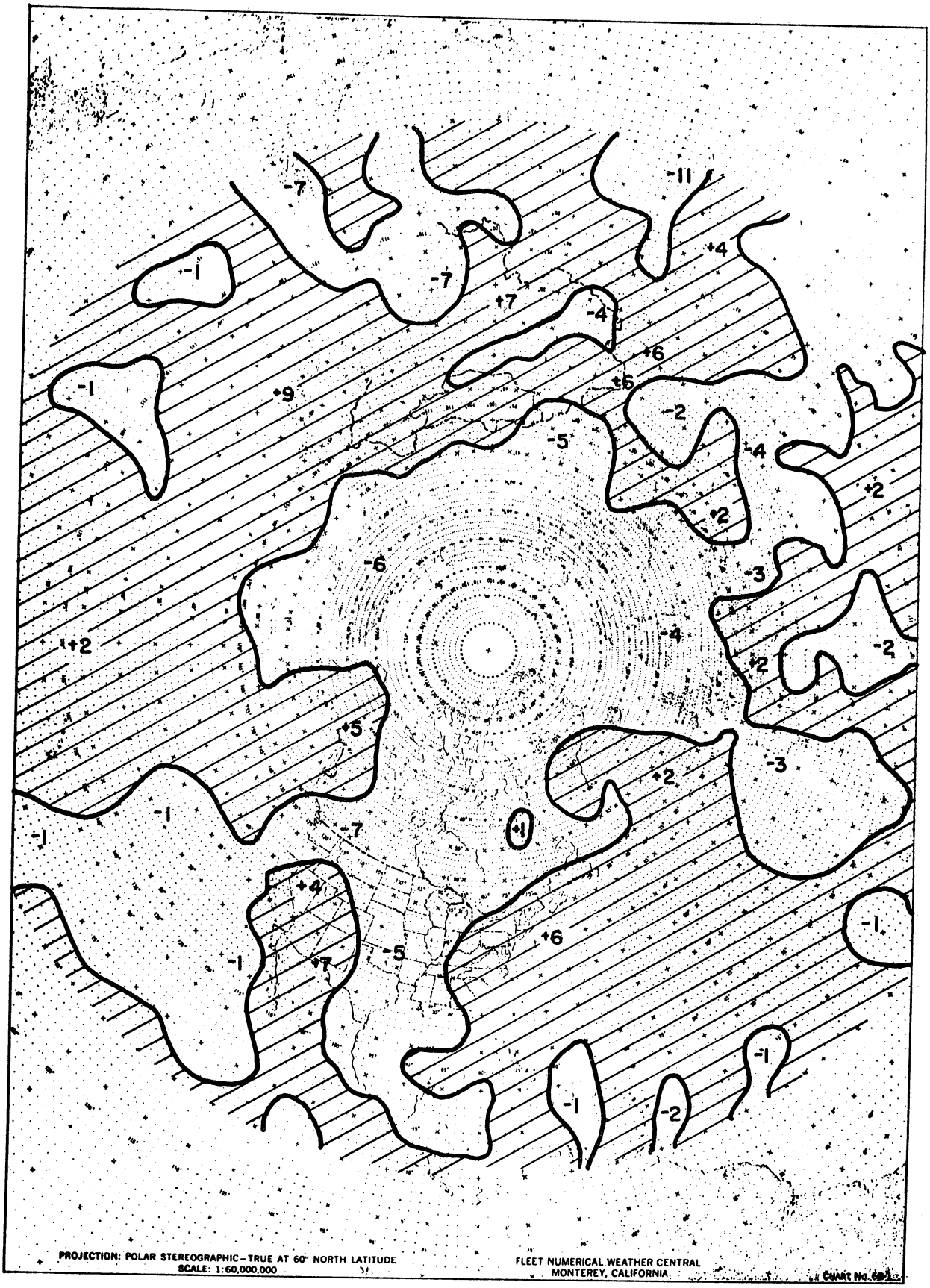

Fig. 9. Monthly average of the diabatic processes at 77.5 cb for January 1969, in the units 10^{-2} kj sec^{-1} ton^{-1}.

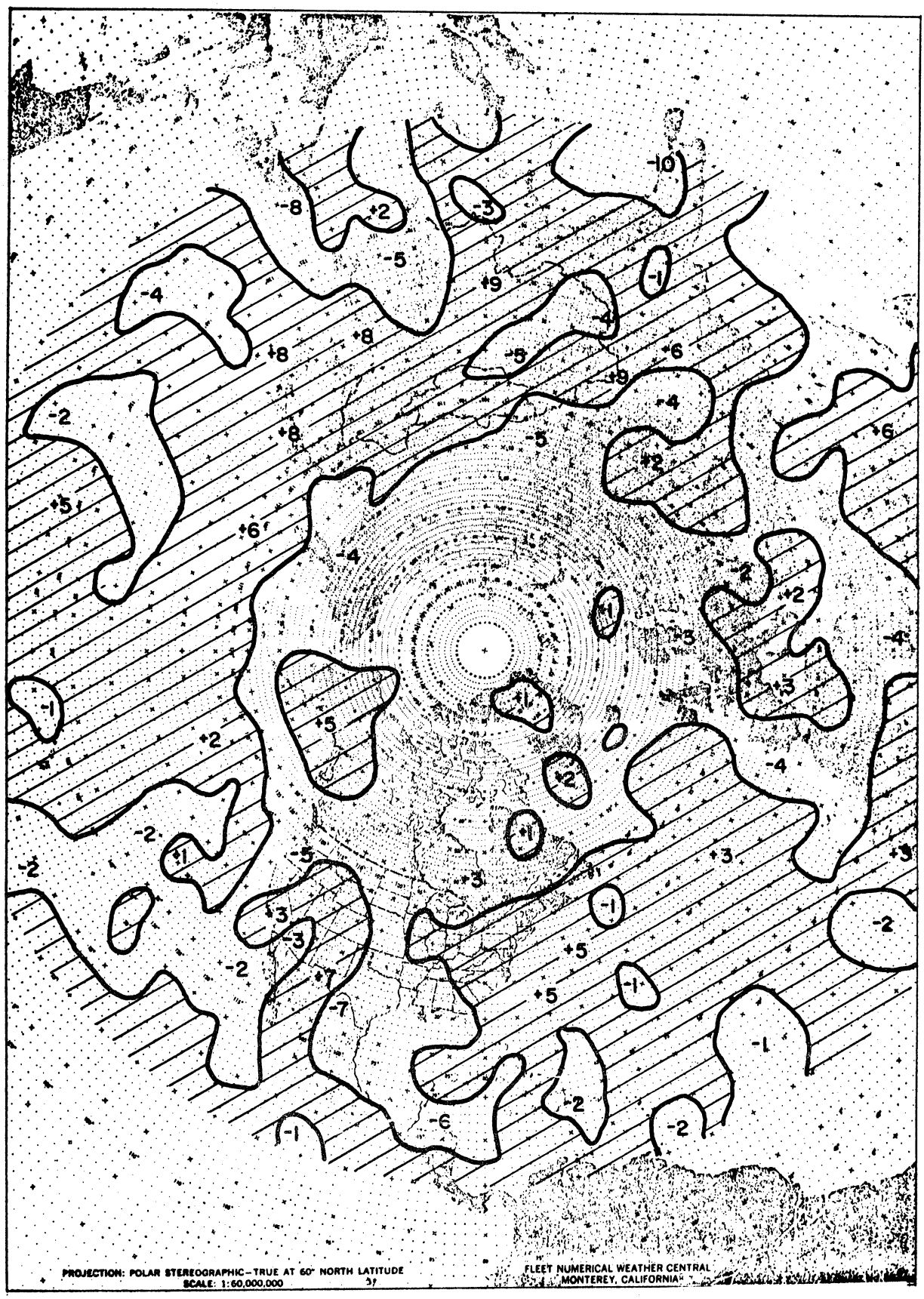

Fig. 10. Monthly average of the diabatic processes at 60 cb for January 1969, in the units 10^{-2} kj sec^{-1} ton^{-1}.

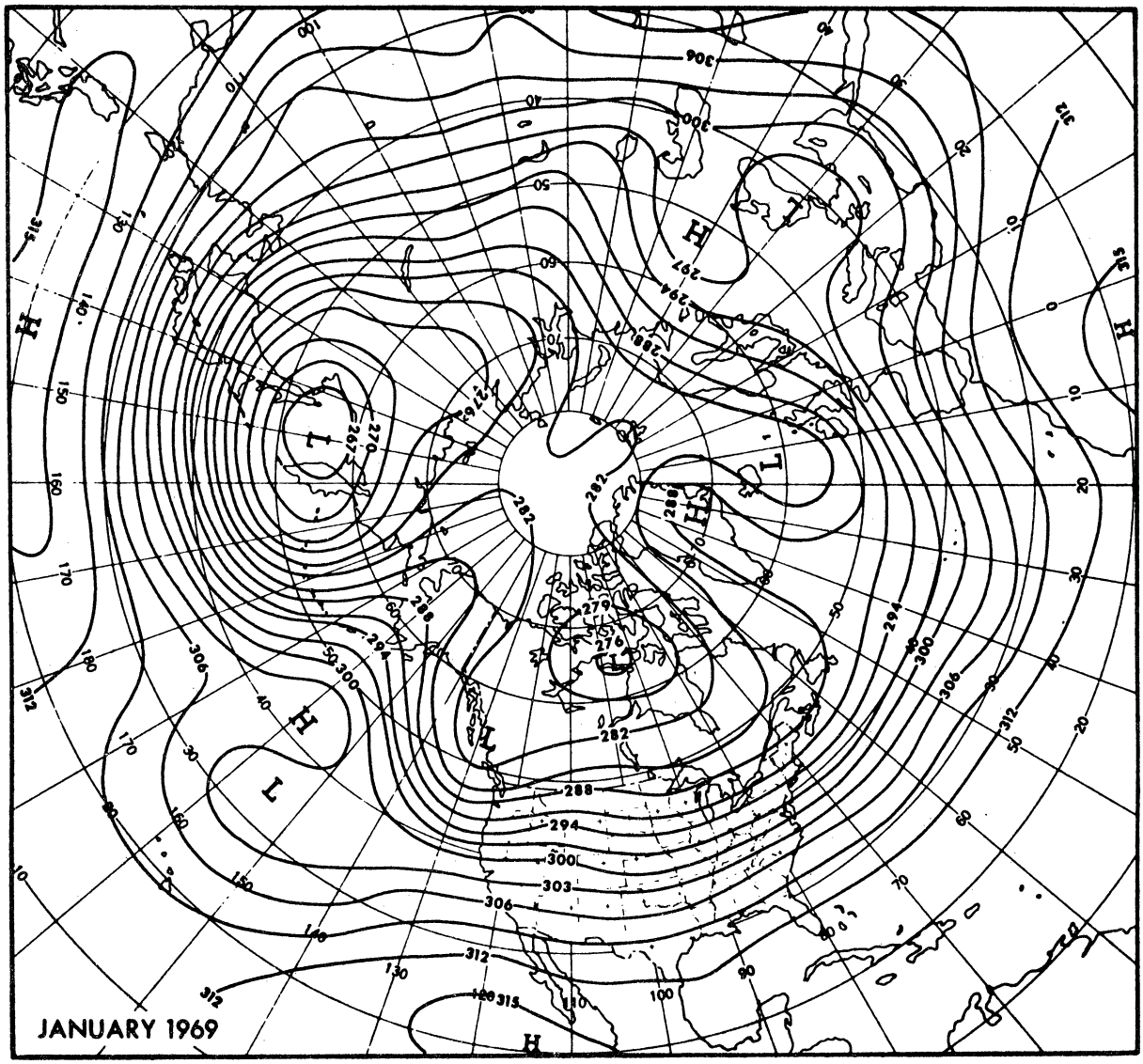

Fig. 11. Mean 70-cb contours (decameters) for January 1969.

100% of normal precipitation for the month. Some western areas received more than 400% of the normal amount. At the same time, sections in the southeastern and southwestern United States accumulated less than 50% of the normal rainfall for the month. Patterns associated with the areas of abundant moisture suggest that the release of latent heat was largely responsible for the heating.

Finally, Figs. 14 and 15 contain the patterns at 45 and 35 cb, respectively. As has been pointed out by Lawniczak (1969), the extensive areas of heating at these levels is the important feature. Since the release of latent heat at these levels would not appear to be very important, the only conclusion seems to be that these areas are the result of the trapping of the outgoing long wave component by average cloudiness. Katayama (1967) and Johnson and Shen (1968) have shown how effective this trapping can be. Heating can result within a layer when the radiation returned by the higher cloud deck causes a net convergence of the long wave component within the layer. An analysis of average cloudiness at various levels might help to explain these features.

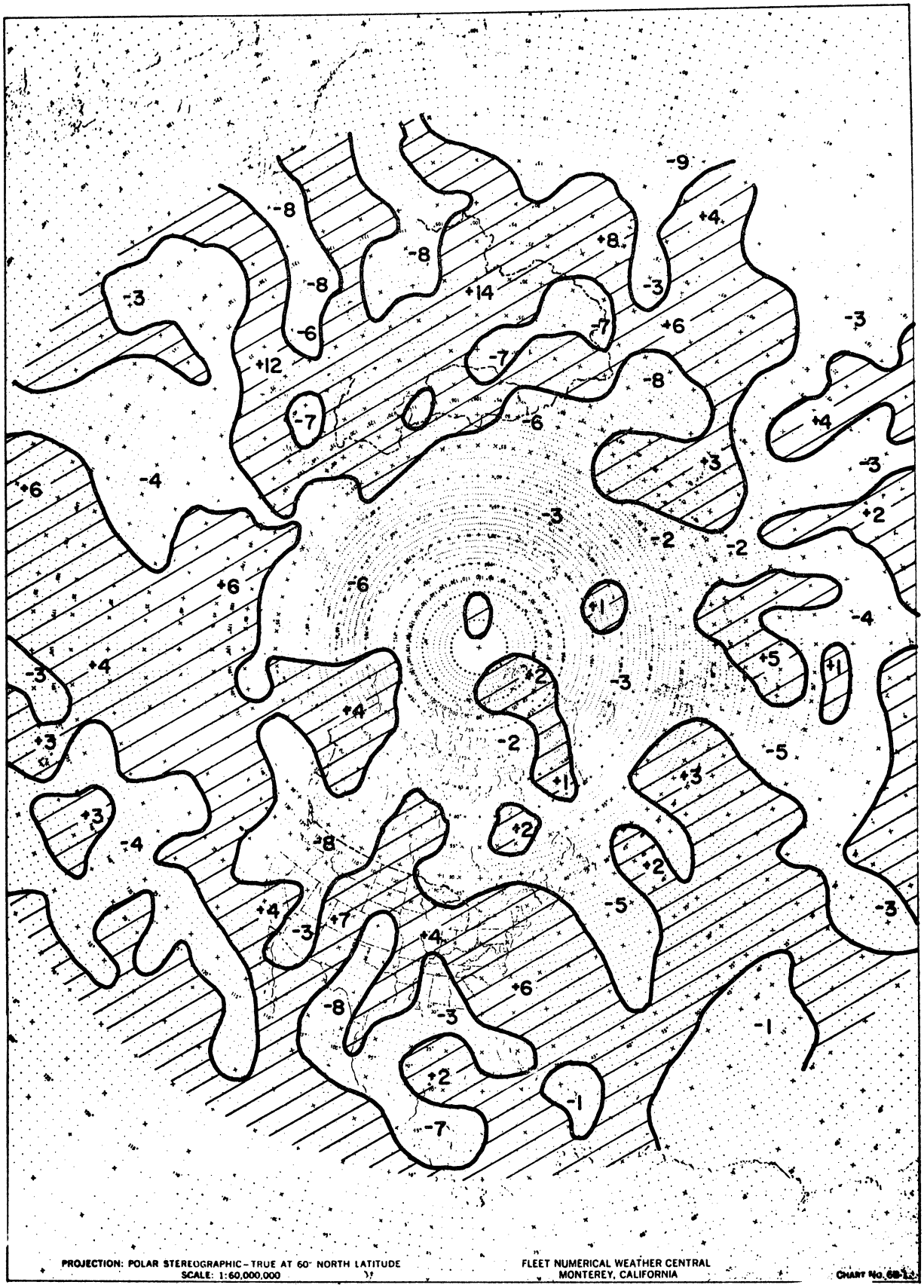

Fig. 12. Monthly average of the diabatic processes at 45 cb for January 1969, in the units 10^{-2} kj sec^{-1} ton^{-1}.

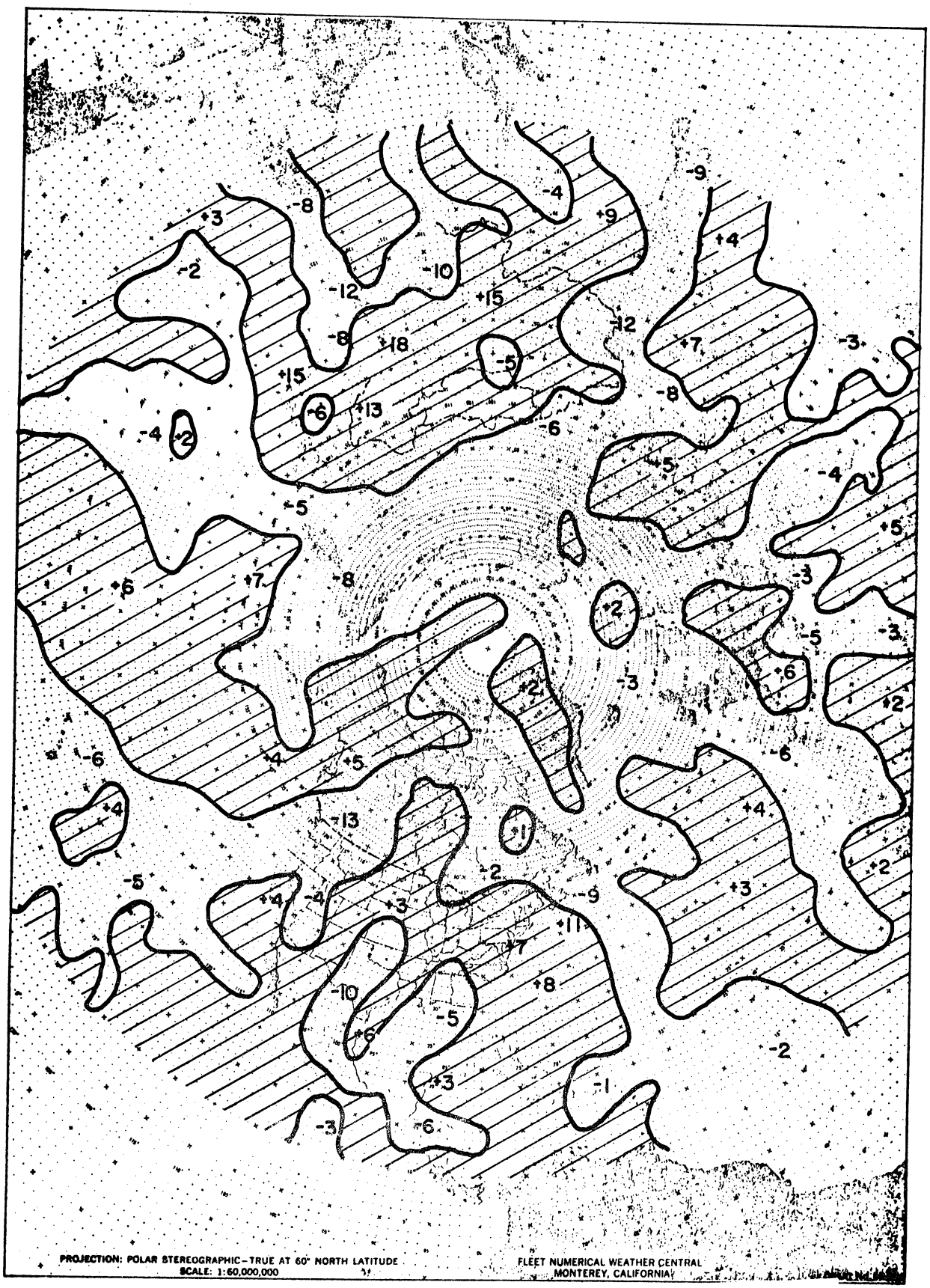

Fig. 13. Monthly average of the diabatic processes at 35 cb for January 1969, in the units 10^{-2} kj sec^{-1} ton^{-1}.

3.3. THE GENERATION OF AVAILABLE POTENTIAL ENERGY

Since the computations of diabatic processes appear reasonable for the layer from 100 to 30 cb and within the area bounded by the latitude circles at 12.5N and 87.5N, calculations for the generation of APE were made using the equations described in Section 2.4. Although (2.23) requires the volume integration over the whole atmosphere, the lack of information over much of the globe makes this impossible. Therefore only the contribution from about 30% of the atmosphere's volume can be measured. Oort (1964a), Smagorinsky, Manabe, and Halloway (1965), Manabe and Smagorinsky (1967), Perry (1967), and Manabe and Hunt (1968) all show that most of the generation of APE occurs in the troposphere. Excluding the stratosphere would not appear to be significant.

In the application of (2.30) and (2.31), the latitudinal band count, k, is equal to 31 since the contributions from the bands centered at 5N, 7.5N, and 10N have been excluded. The diabatic fields at 92.5, 77.5, 60, 45, and 35 cb are considered to be representative for their respective layers. Grid-point analyses of the diabatic processes and the layer thicknesses were transformed into latitude bands of 2.5 deg width containing 256 points using bi-linear interpolation. These bands were then separated into Fourier components using harmonic analysis and only the first fifteen wave components and the mean were used in the computations for the generation of APE. Diabatic and thickness analyses are available at twelve-hourly intervals from 1200, GMT 1 January through 0000 GMT 31 January. Likewise, the computations for the generation of APE cover the same period with the same interval. Individual results for each set were then averaged over the period in order to obtain the means.

3.4. THE GENERATION OF APE AS A FUNCTION OF LATITUDE AND PRESSURE FOR THE LAYER FROM 100 TO 30 cb

The monthly average of the generation of zonal APE as a function of latitude for the layer from 100 to 30 cb is plotted in Fig. 14 where the units are 10^{-4} kj m^{-2} sec^{-1} and the values are related to the areas of their respective latitude bands. Each band's contribution involves an area weighting factor which obviously has a greater value in the lower latitudes. For example, the area for the band centered at 30N is larger than the area for the band at 60N by a factor of about 1.7.

An obvious result shown in Fig. 14 is that the plotted values are mostly positive. This means that on the average the zonal processes are positively correlated. Diabatic heating therefore takes place in the warm low latitudes and diabatic cooling occurs in the colder polar latitudes. The negative region between 35N and 50N exists because the transition zones for the area deviations of both the diabatic processes and the temperature field do not coincide. As Fig. 14 shows, the major contribution toward the generation of zonal APE comes from the area north of 50N. The small contribution in the tropical latitudes is of course related to the smaller net heating in this region as shown in Fig. 6.

Table 1 contains the tabulation of the data shown in Fig. 14 along with the standard deviation for each latitude band. Variability about the mean on a day-to-day basis is of course indicated by the magnitude of the standard deviation. Since weather phenomena are quite changeable about the globe on a day-to-day basis, such variations about the mean are understandable. In all probability, these variations are mostly indicative of weather behavior and not

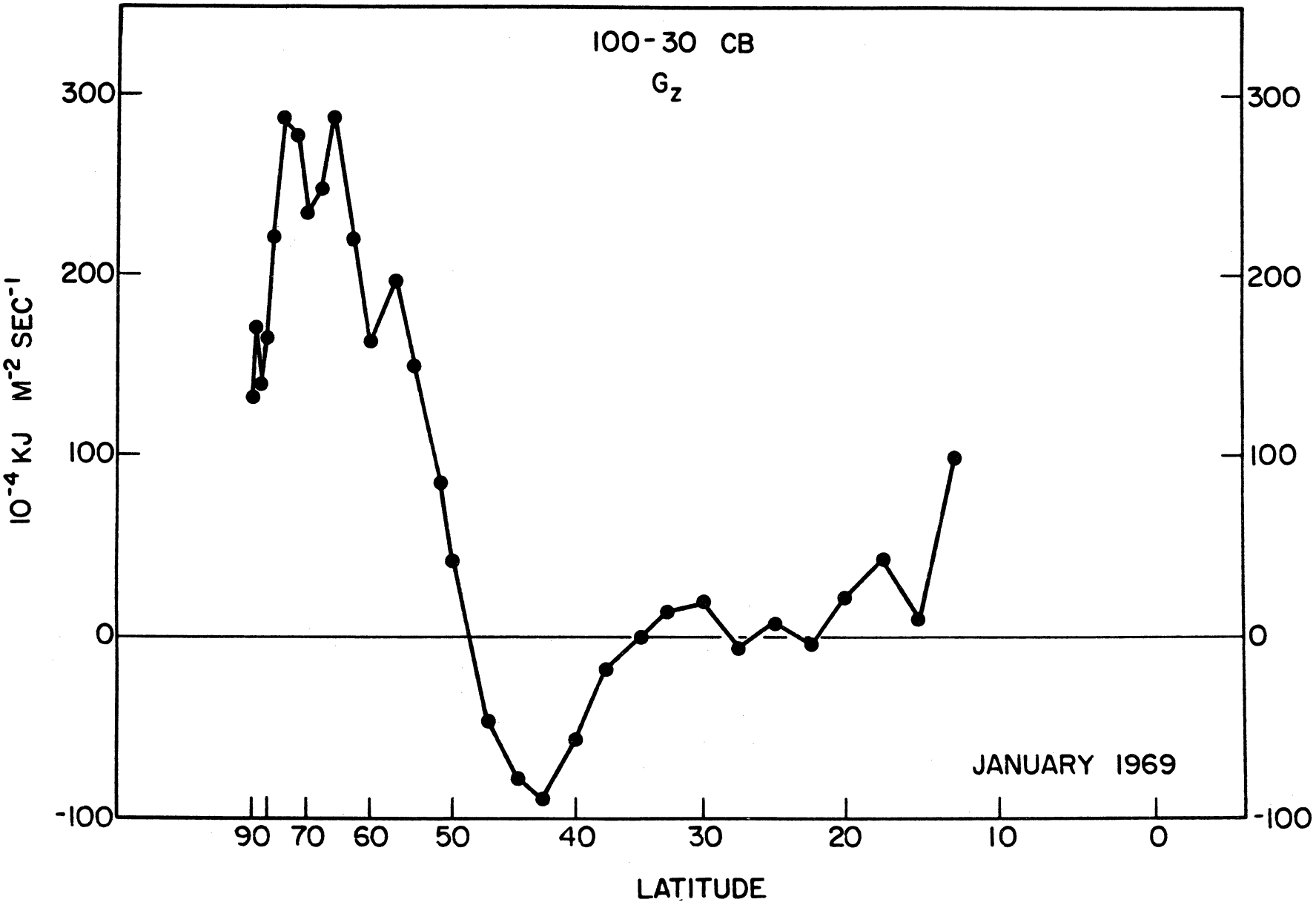

Fig. 14. Monthly average of the generation of zonal APE as a function of sine of the latitude for the layer from 100 to 30 cb for January 1969.

TABLE 1

LATITUDINAL VARIATION OF THE GENERATION OF ZONAL AVAILABLE POTENTIAL ENERGY IN THE LAYER 100-30 cb COMPUTED FOR THE RING CENTERED AT THE INDICATED LATITUDE IN UNITS 10^{-4} kj m^{-2} sec^{-1} FOR JANUARY 1969

Latitude	G_z	Standard Deviation
12.5	100.2	96.6
15.0	10.1	65.5
17.5	43.2	59.6
20.0	22.0	54.8
22.5	- 3.7	60.1
25.0	7.6	38.9
27.5	- 5.6	30.8
30.0	18.7	28.1
32.5	13.8	19.8
35.0	0.3	5.7
37.5	- 17.4	22.3
40.0	- 55.8	50.4
42.5	- 89.1	68.2
45.0	- 77.3	83.1
47.5	- 45.6	98.9
50.0	42.7	123.5
52.5	85.5	163.0
55.0	149.4	157.0
57.5	197.4	144.1
60.0	162.4	172.1
62.5	219.8	137.3
65.0	287.9	152.7
67.5	248.2	184.9
70.0	234.2	184.3
72.5	278.6	170.0
75.0	287.0	192.0
77.5	220.7	206.0
80.0	164.6	265.2
82.5	139.5	280.9
85.0	170.0	320.7
87.5	132.6	461.2

of basic analysis uncertainties and errors.

Assuming normal distribution, generation of zonal APE occurred between 55N and 80N most of the time. The very large standard deviations north of 80N are most likely associated with the small area of this region in which weather systems can exchange roles within short-time periods. The bands near 40N were nearly always destructive of zonal APE while the tropical areas show much variability. An analysis of the calculations within individual layers shows that the same general results apply with the exception that in the two layers above 50 cb, only the band centered at 57.5N had a standard deviation smaller than the magnitude of the mean value.

Average monthly results for the generation of eddy APE are shown in Fig. 15. Here an obvious result is that the values are almost totally negative which means that, on the average, warm eddies were cooled and cold eddies were warmed. Maximum destruction of eddy APE occurred between 40N and 50N which suggests that the baroclinic processes associated with the polar front are responsible. Again assuming normal distribution, Table 2 indicates that destruction of eddy APE took place most of the time between 30N and 50N. However, an examination of the results within the individual layers reveals that above 70 cb, there were essentially no layers in which the standard deviation was less than the magnitude of the mean value for any latitude band. Thus the maximum destruction is associated with the lowest 30 cb of the atmosphere and most likely the release of latent heat and the trapping effects of clouds in the warm eddies act to produce the variability in the higher layers.

Finally in the latitude bands south of 20N, net generation of eddy APE occurred and appears to have taken place most of the time near 15N. The

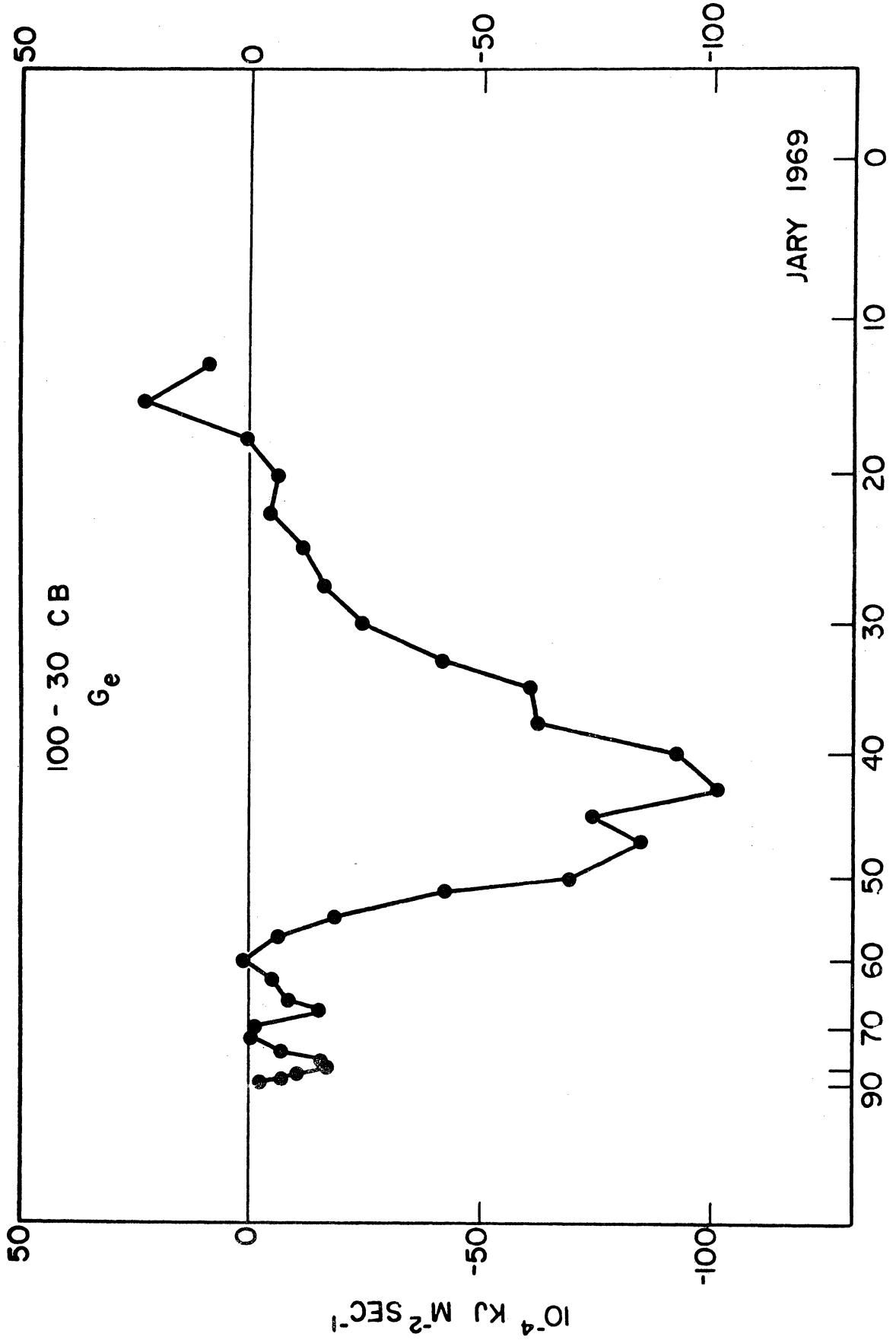

Fig. 15. Monthly average of the generation of eddy APE as a function of sine of the latitude for the layer from 100 to 30 cb for January 1969.

TABLE 2

LATITUDINAL VARIATION OF THE GENERATION OF EDDY AVAILABLE POTENTIAL ENERGY IN THE LAYER 100-30 cb COMPUTED FOR THE RING CENTERED AT THE INDICATED LATITUDE IN UNITS 10^{-4} kj m^{-2} sec^{-1} FOR JANUARY 1969

Latitude	G_e	Standard Deviation
12.5	9.2	14.5
15.0	22.9	13.3
17.5	1.0	9.0
20.0	- 5.9	11.2
22.5	- 4.1	15.7
25.0	- 11.4	17.2
27.5	- 15.9	24.5
30.0	- 24.3	22.1
32.5	- 41.7	29.9
35.0	- 60.6	48.1
37.5	- 62.3	53.6
40.0	- 92.1	78.7
42.5	-101.0	60.2
45.0	- 74.2	62.3
47.5	- 84.6	66.7
50.0	- 69.0	58.3
52.5	- 42.2	50.7
55.0	- 18.4	44.9
57.5	- 6.9	39.0
60.0	1.4	41.4
62.5	- 4.6	52.3
65.0	- 8.2	56.6
67.5	- 15.1	48.2
70.0	- 0.8	29.8
72.5	- 0.3	28.1
75.0	- 7.0	35.6
77.5	- 16.5	38.8
80.0	- 16.8	35.2
82.5	- 10.4	23.5
85.0	- 6.6	18.2
87.5	- 2.2	8.3

magnitudes are much smaller there than in the mid-latitudes but again the generation appears to be the result of processes at work in the lowest 30 cb.

A comparison of the average generation of zonal and eddy APE for the month as a function of the pressure layers used in the calculation is shown in Figs. 16 and 17, respectively. The units are 10^{-6} kj m^{-2} sec^{-1} cb^{-1} and the area covered extends from 11.25N to 88.75N. The generation of zonal APE was essentially a constant for the troposphere while significant destruction of eddy APE occurred in the lowest 30 cb. Strong cooling of clear and cold air masses coupled with cloud and latent heat effects in the warm air would reduce the net destruction in the higher layers. Table 3, which lists the standard deviations, shows that more variability is associated with the higher layers for both zonal and eddy APE. For the troposphere, about 70% (80%) of the total contribution to the generation of zonal (eddy) APE occurred in the lowest 50 cb.

TABLE 3

LAYER VARIATION OF THE GENERATION OF ZONAL AND EDDY AVAILABLE POTENTIAL ENERGY FOR THE REGION FROM 11.25N TO 88.75N IN THE UNITS 10^{-6} kj m^{-2} sec^{-1} cb^{-1} FOR JANUARY 1969

Layer	G_z	Standard Deviation	G_e	Standard Deviation
100 - 85 cb	80.2	34.2	-54.0	25.7
85 - 70 cb	82.3	24.4	-53.5	18.4
70 - 50 cb	75.4	30.6	-32.5	19.5
50 - 40 cb	74.4	46.9	-27.9	20.9
40 - 30 cb	80.0	55.9	-37.0	33.6

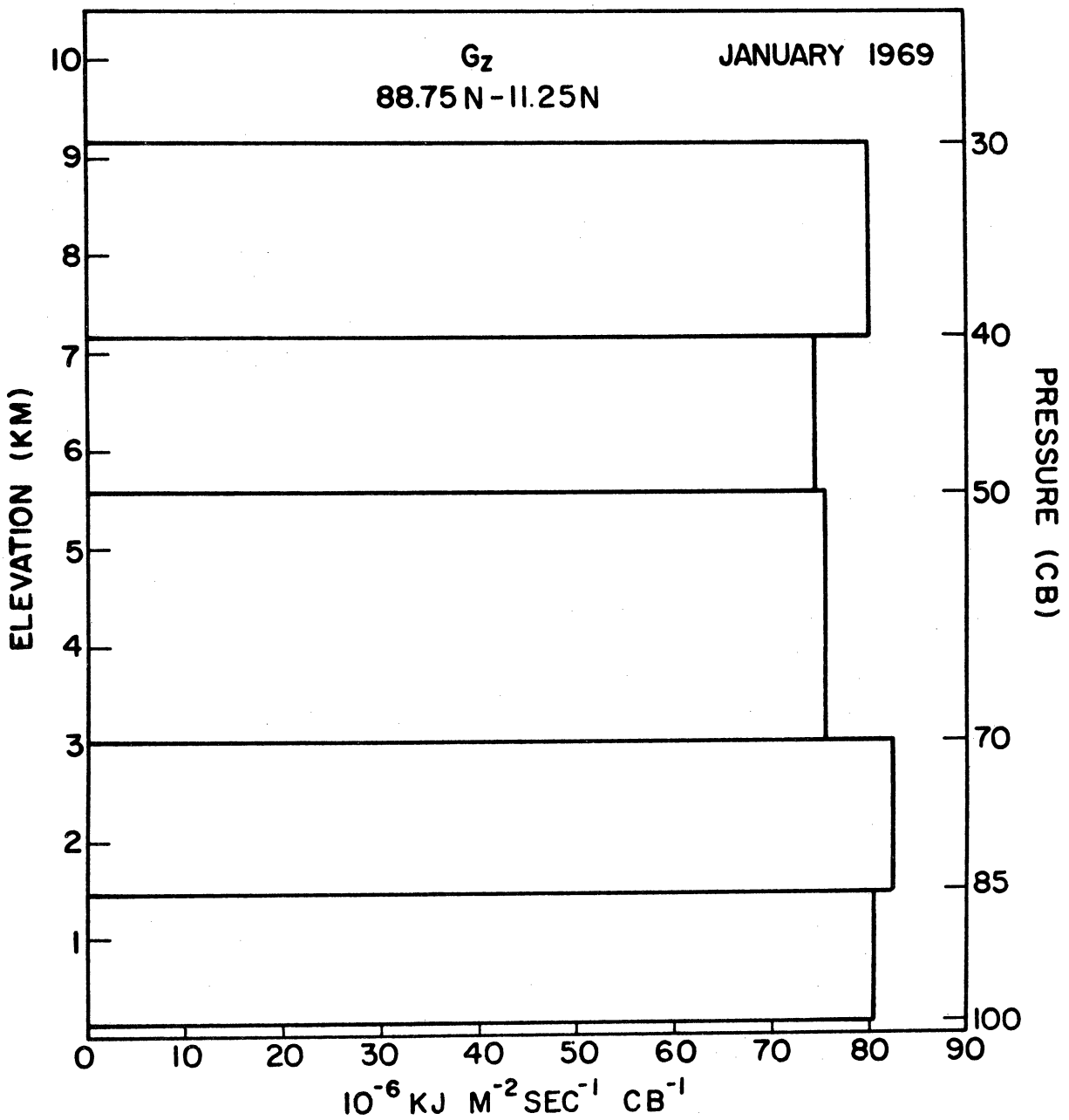

Fig. 16. Monthly average of the generation of zonal APE as a function of pressure layers for January 1969.

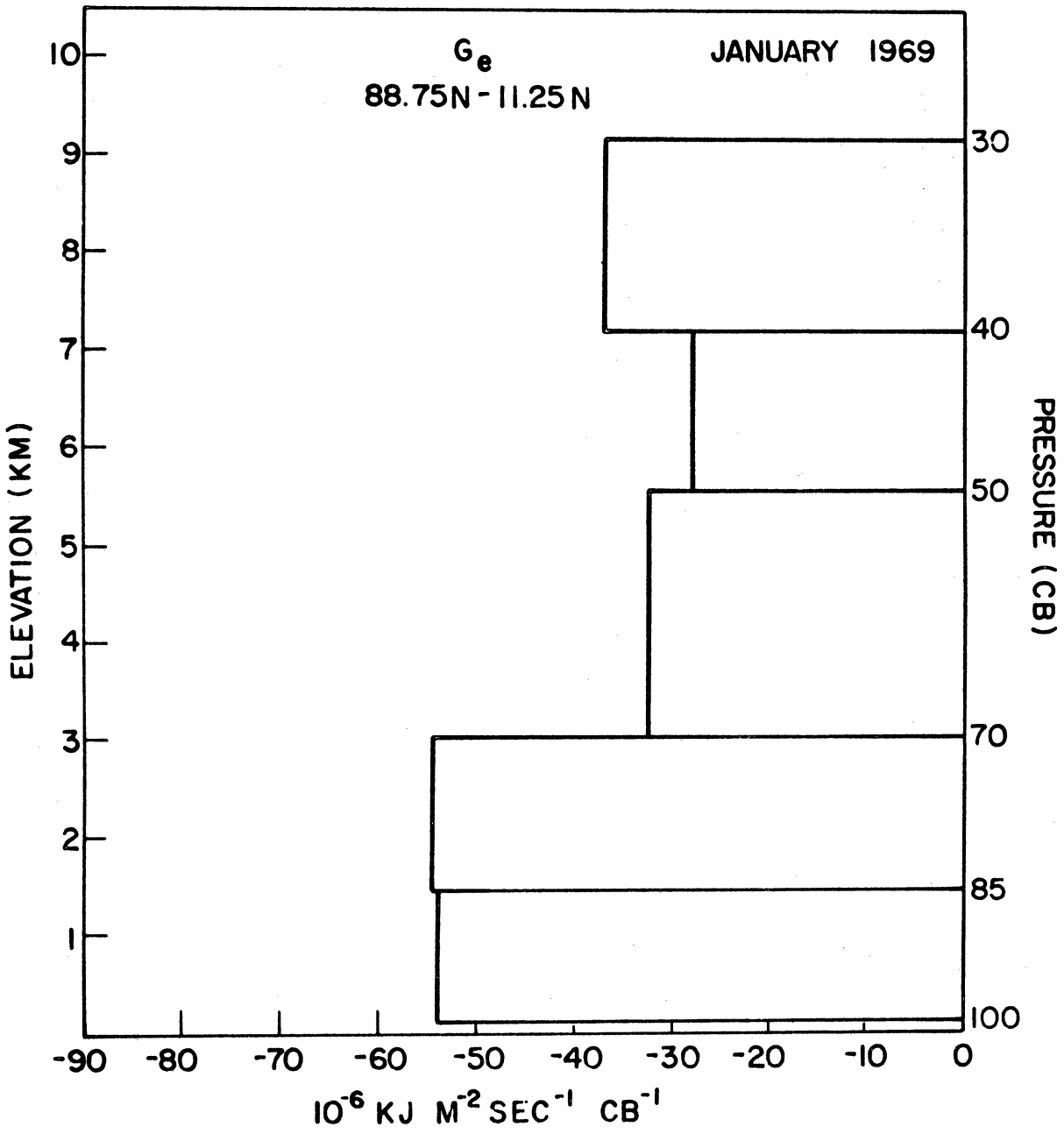

Fig. 17. Monthly average of the generation of eddy APE as a function of pressure layers for January 1969.

3.5. GENERATION OF EDDY APE BY WAVE NUMBER

Fourier coefficients calculated by harmonic analysis were used to determine the importance of the individual waves in generating or destroying eddy APE. Figure 18 presents the average of the daily values for the layer from 100 to 30 cb while Table 4 lists the data and the standard deviations. Clearly, the dominant modes involved in destroying eddy APE within the troposphere are the long and medium waves, particularly waves 1 and 4. Lack of sufficient data over much of the hemisphere prevents a meaningful analysis of the importance of the shorter waves.

TABLE 4

HARMONIC ANALYSIS OF THE GENERATION OF EDDY AVAILABLE POTENTIAL ENERGY IN THE LAYER 100-30 cb FOR THE REGION FROM 11.25N to 88.75N IN THE UNITS 10^{-4} kj m^{-2} sec^{-1} FOR JANUARY 1969

Wave Number	Average	Standard Deviation
1	-6.2	5.1
2	-3.6	6.9
3	-3.0	3.2
4	-5.5	4.4
5	-3.3	5.0
6	-2.1	2.4
7	-3.6	3.3
8	-1.3	1.8
9	-0.5	1.4
10	-0.1	1.1
11	-0.2	0.8
12	-0.0	0.5
13	-0.1	0.5
14	0.1	0.5
15	0.2	0.4

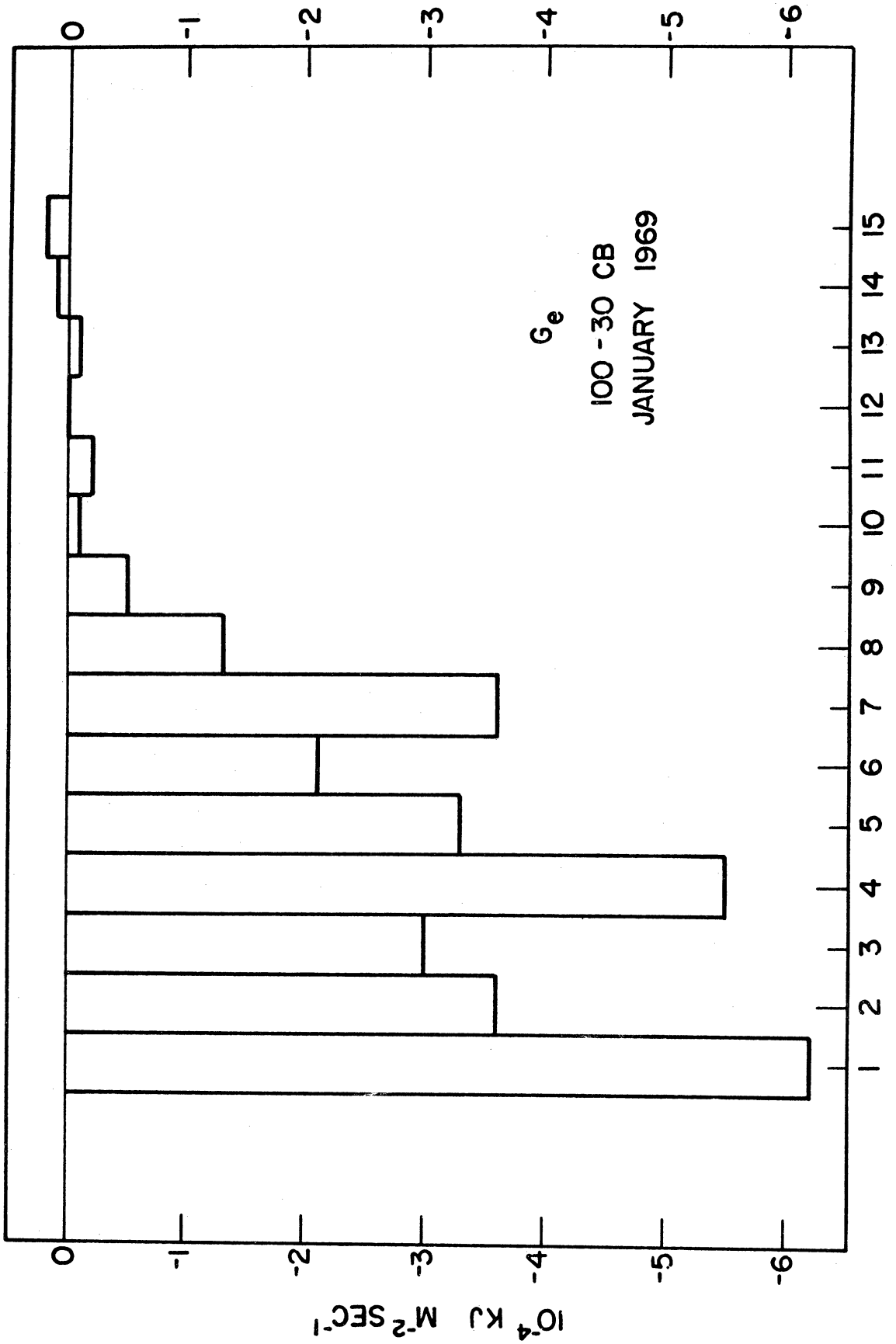

Fig. 18. Monthly average of the individual wave contribution for the generation of eddy APE for the layer from 100 to 30 cb for January 1969.

Figure 19 depicts the wave contribution as a function of the individual layers. While wave 4 is the dominant mode for the top and bottom layers, wave 1 is dominant from 85 cb to 40 cb.

3.6. THE NET RESULTS OF THE GENERATION OF APE

Data limitations and the small sample size only justify the highlights presented in this chapter. On the basis of the calculations described, on the average for January 1969, zonal APE was generated at a rate of 55×10^{-4} kj sec^{-1} m^{-2} with a standard deviation of 20 units while eddy APE was destroyed at a rate of 29×10^{-4} kj sec^{-1} m^{-2} with a standard deviation of 12 units.

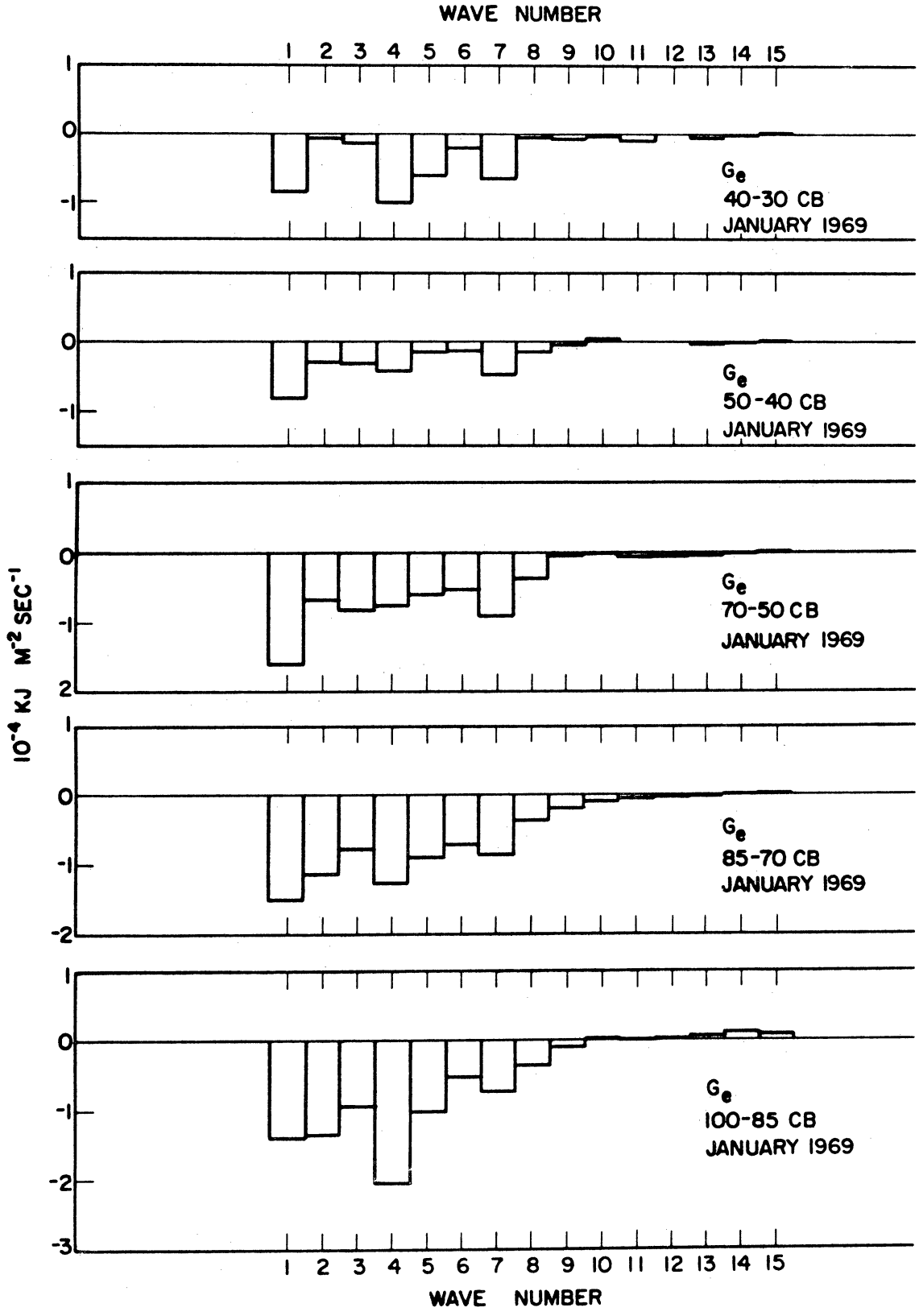

Fig. 19. Monthly averages within the indicated layers for the individual wave contributions to the generation of eddy APE for January 1969.

CHAPTER 4

SUMMARY AND SUGGESTIONS

4.1. CONCLUSIONS

This study has examined results of the calculations of diabatic processes and the generation of available potential energy. Computations were made over the Northern Hemisphere between 11.25N and 88.75N in the layer from 100 to 30 cb for January 1969. The input data consisted of the grid-point values from the Fleet Numerical Weather Central (FNWC) daily objective height analyses at six levels within this layer. Diabatic processes were calculated using a five-layer quasi-geostrophic model in which the lower boundary processes and the vertical changes of the total derivative (horizontal) of geostrophic potential vorticity are computed. As a result, for the first time much better resolution of the vertical structure of the diabatic processes and the generation of APE, based on atmospheric observational data over much of the Northern Hemisphere, is available. The model further includes a more realistic treatment of the lower boundary effects. Specifically, the variable terrain height data due to Berkofsky and Bertoni (1955) and Cressman's (1960) drag coefficients are used to calculate the lower boundary vertical velocities and frictional effects. Also, in accordance with quasi-geostrophic theory, static stability is allowed to vary with pressure.

Use of the FNWC analyses eliminated the boundary problems encountered with the National Meteorological Center's analyses in a previous study by Lawniczak (1969). However, due to the nature of the quasi-geostrophic assumption, there is a practical boundary imposed as a result of the sine's smaller values at low

latitudes. Failure of the model in the high troposphere and stratosphere has been discussed by Lawniczak (1969). Since the product of the square of the Rossby number with the Richardson number must be of order one in quasi-geostrophic theory, the existence of a maximum wind level or a very stable region invalidates this relationship and likewise the theory. Thus only the results in about 30% of the earth's atmosphere are available for analysis in this study. However, based on previous studies, the elimination of the stratosphere does not appear to be significant.

Monthly mean values of the diabatic processes in the layer from 100 to 30 cb indicate that the change of surface cover to permanent snow or ice-cover is quite effective in separating the mean heating region from the mean cooling region in the troposphere. For January 1969, this separation occurred near 50N and extended almost vertically above this latitude throughout the troposphere. Maximum heating (cooling) was calculated near 40N (70N) in the lower troposphere. Low heating values in the tropics suggests that there is a near balance between the long wave radiational cooling component and the heating due to solar absorption, latent heat release, and the boundary flux.

The averages for the individual levels reveal the complexities involved when dealing with the net effect of the diabatic processes. In particular, although it would seem that the long wave component should dominate the layers above 50 cb everywhere in the high troposphere and low stratosphere, the average heating patterns found at 45 and 35 cb suggest otherwise. Apparently the existence of regions of average high cloudiness is required in order to trap the long wave emission and thus warm the layers beneath the cloud bases.

Using the daily values of the diabatic processes in the five layers from

100 to 30 cb, the daily generation of APE was calculated. For January 1969, the average generation of zonal APE was 55×10^{-4} kj m^{-2} sec^{-1} and eddy APE was destroyed at the rate of 29×10^{-4} kj m^{-2} sec^{-1}. It may be that only fortuitous circumstances produced the very favorable comparison with the value obtained by Dutton and Johnson (1967) for the generation of zonal APE. However, their results represent an average for the year while only one month's results are presented here. Needless to say, additional calculations on a larger data set are required. But these results indicate that heating (cooling) takes place in lower (higher) latitudes and warm (cold) eddies are cooled (heated) everywhere on the average.

In the region analyzed, on the average, a substantial amount of the generation of zonal APE and the destruction of eddy APE occurred in the lowest 30 cb of the troposphere. (Although Lawniczak (1969) obtained a near balance between these components in lowest layer for March 1963, this was not true for these results.) Polar latitudes contributed most to the generation of zonal APE while the baroclinic activity associated with the polar front apparently led to the maximum destruction of eddy APE near 40N in the lower troposphere. The relase of latent heat in the warm sector and differential cooling effects due to clouds apparently reduce the net destruction of eddy APE above 70 cb.

Harmonic analysis reveals that the long and medium waves were most important in destroying eddy APE. Very little energy transformation occurred in the shorter waves. But since the observational data are not adequately distributed, the exact role of the shorter waves remains indistinct. For January 1969, waves 1 and 4 were the dominant destructive modes when the whole regime was considered while wave 4 was the significant destructive mode for the layers

from 100 to 85 cb and 40 to 30 cb while wave 1 was dominant in the other layers.

4.2. SUGGESTIONS FOR FUTURE RESEARCH

A very serious problem confronting observational studies is the lack of adequate data on a global basis. The problem is no less serious at the hemispheric level. Figures 2 and 3 show how inadequate the data coverage is over the oceanic regions and the land areas south of about 30N. But it will be some time before this situation improves. And finally, it remains to be determined what constitutes the "best" analysis of the mass-structure of the atmosphere.

The use of the variable lower boundary values at a fixed pressure level was made in this study. It is true that the number of grid points at which the pressure at terrain height is lower than 85 cb is small. Nevertheless, a comparison utilizing these diabatic effects as a function of terrain-height pressure should be made.

It very well may be that no simple theory exists by which the diabatic processes in the higher atmosphere can be determined diagnostically. The increasing data being made available through the efforts of the aeronomers may eventually allow computations to be made in this regime. Although the present study implies that most of the important results occur in the troposphere, the inquiry should be expanded as soon as practicable to include the stratosphere and to verify its exact role.

APPENDIX

FINITE DIFFERENCE FORMS OF THE EQUATIONS

A.1. BASIC INFORMATION

The finite difference forms of the equations used in the calculations for the diabatic processes are provided in this appendix. All standard symbols are explained in the list near the beginning of this paper. Figure 20 shows the computational grids required to locate the necessary points. The upper diagram is required only for the vertical differentiation needed in calculating the geostrophic potential vorticity while the lower diagram applies to the horizontal operators. Also, the relevant equation number from the text is given where it is appropriate.

As for the finite differencing scheme itself, consider some f(x) where

$$f(x \pm \Delta x) = f(x) \pm f'(x)\Delta x \pm f''(x) \frac{\Delta x^2}{2} \pm \ldots \quad . \tag{1}$$

Subtracting the two series represented by (1) leads to

$$f'(x) = \frac{f(x + \Delta x) - f(x - \Delta x)}{2\Delta x} + O(\Delta x)^2 \quad , \tag{2}$$

which is a centered difference formula for the first derivative. The order of the remainder, in this case $(\Delta x)^2$, is a measure of the accuracy of the approximation. Usually, the higher the order, the better the approximation is.

Adding the two series in (1) gives the centered difference form for the second derivative,

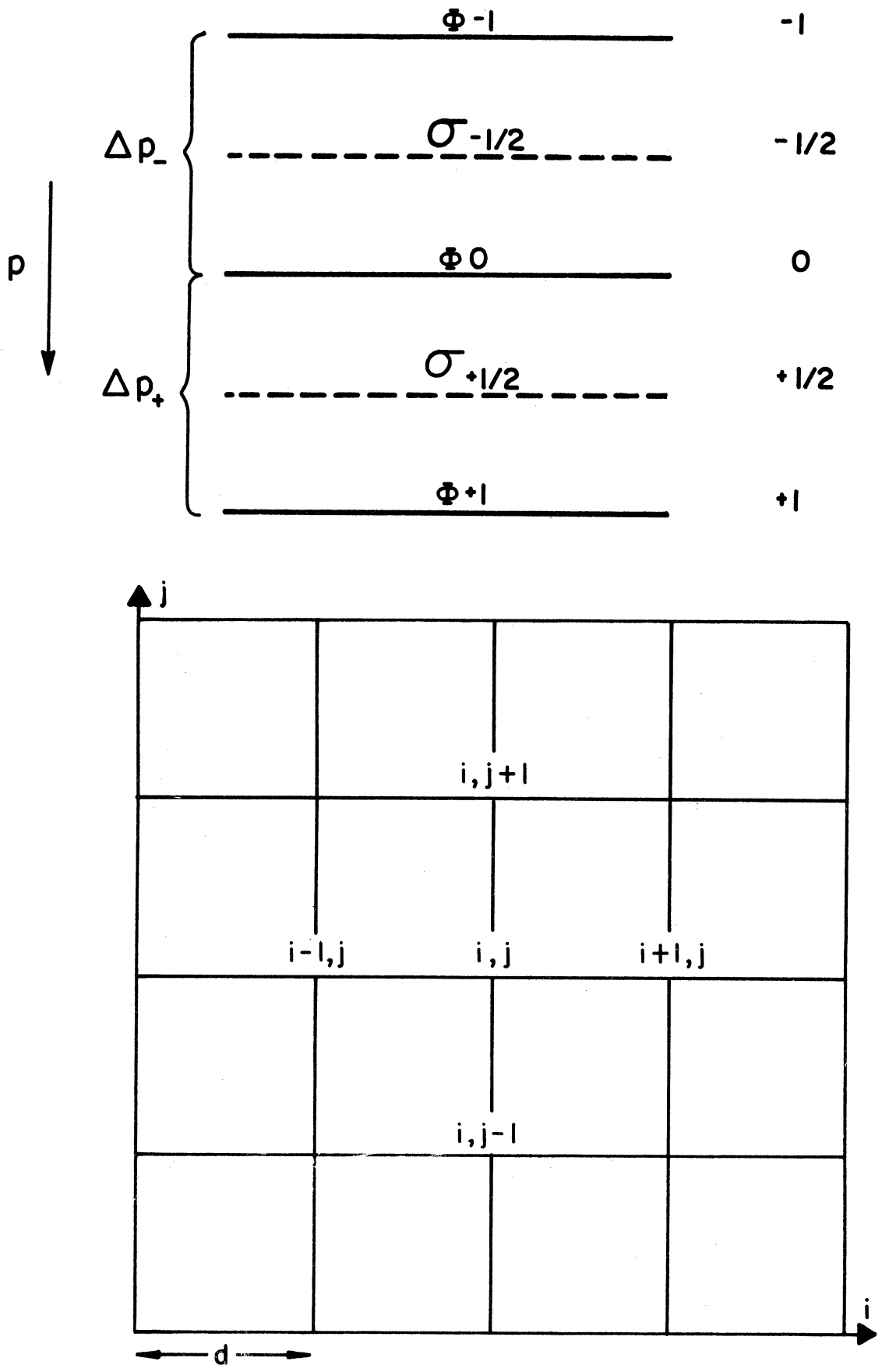

Fig. 20. Vertical and horizontal finite differencing grids.

$$f''(x) = \frac{f(x+\Delta x) - 2f(x) + f(x-\Delta x)}{\Delta x^2} + O(\Delta x)^2 \quad . \tag{3}$$

Since the material presented in this study is diagnostic in nature, computational instability associated with a time-stepping or prediction procedure is not a problem. But since the centered differences have remainders of higher order than either forward or backward differences, they are to be preferred and will be used. Round-off errors due to the physical storage capacity of the computer and truncation errors due to the differencing scheme can be problems. However, nothing can be done about the former and so long as Δx is sufficiently small when compared to the characteristic horizontal scale of the problem, the latter is negligible.

A.2. GEOSTROPHIC POTENTIAL VORTICITY, (2.6)

The geostrophic potential vorticity is calculated using

$$\xi_o = \frac{m^2}{fd^2} \nabla^2 \Phi + f + \frac{2\bar{f}}{\Delta p_+ + \Delta p_-} \left[\frac{\Phi_1 - \Phi_o}{\sigma_{\frac{1}{2}} \Delta p_+} - \frac{\Phi_o - \Phi_{-1}}{\sigma_{-\frac{1}{2}} \Delta p_-} \right] \tag{4}$$

where $\nabla^2() = ()_{i+1,j} + ()_{i,j+1} + ()_{i-1,j} + ()_{i,j-1} - 4()_{i,j}$.

A.3. LOCAL TIME DERIVATIVE OF GEOSTROPHIC POTENTIAL VORTICITY

Using a centered finite difference over 24 hr, the local time change of the geostrophic potential vorticity is calculated from

$$\frac{\partial \xi}{\partial t} = \frac{\xi_{+12} - \xi_{-12}}{8.64 \times 10^4} \quad . \tag{5}$$

Likewise, all other quantities in (2.8), although capable of being computed at observation time, will be averaged over a 24-hr period using

$$()_t = \frac{\left[()_{-12} + 2()_o + ()_{+12}\right]}{4} \quad . \tag{6}$$

A.4. HORIZONTAL ADVECTION

Advection using the geostrophic wind is computed using

$$\begin{aligned}(\vec{V}\cdot\nabla\{\}) = \frac{m^2 g}{4d^2\bar{f}} \Big[&(z_{i+1,j} - z_{i-1,j})(\{\}_{i,j+1} - \{\}_{i,j-1}) - \\ &- (z_{i,j+1} - z_{i,j-1})(\{\}_{i+1,j} - \{\}_{i-1,j})\Big] \quad .\end{aligned} \tag{7}$$

A.5. DEPARTURE VALUE AT THE TERRAIN HEIGHT

Consider a grid point at which the terrain height is related to the heights of two bounding pressure levels such that

$$z_{p_U} > z_o > z_{p_L} \tag{8}$$

Letting D represent the difference between the standard height and the actual height of a pressure level, called the departure value, then the specific temperature anomaly for the bounding layer can be written

$$ST = \frac{D_U - D_L}{Z_{p_U} - Z_{p_L}} \tag{9}$$

Since the anomaly is the mean value for the layer, then

$$D_o = D_U - ST(Z_{p_U} - Z_{p_o}) \quad . \tag{10}$$

But the standard height is determined from

$$Z_{p_o} = z_o - D_o \quad . \tag{11}$$

Therefore, (10) becomes

$$D_o = \frac{D_U - ST(Z_{p_U} - Z_o)}{1 + ST} \quad . \tag{12}$$

A.6. PRESSURE AT TERRAIN HEIGHT

From the results of (12) and knowing Z_{p_o} from (11), using an interpolating polynomial, the pressure at the terrain height is calculated from

$$p_o = \frac{[y(a + by)^2 + u(c + du^2)]}{10} \tag{13}$$

where

$$a = 724.64$$

$$b = 3.5562$$

$$c = 597.37$$

$$d = 3.1272$$

$$u = \frac{Z_{p_o} - 2.7 \times 10^3}{1.5 \times 10^3}$$

and

$$y = 1 - u \quad .$$

Figure 21 depicts the mean of the daily computations.

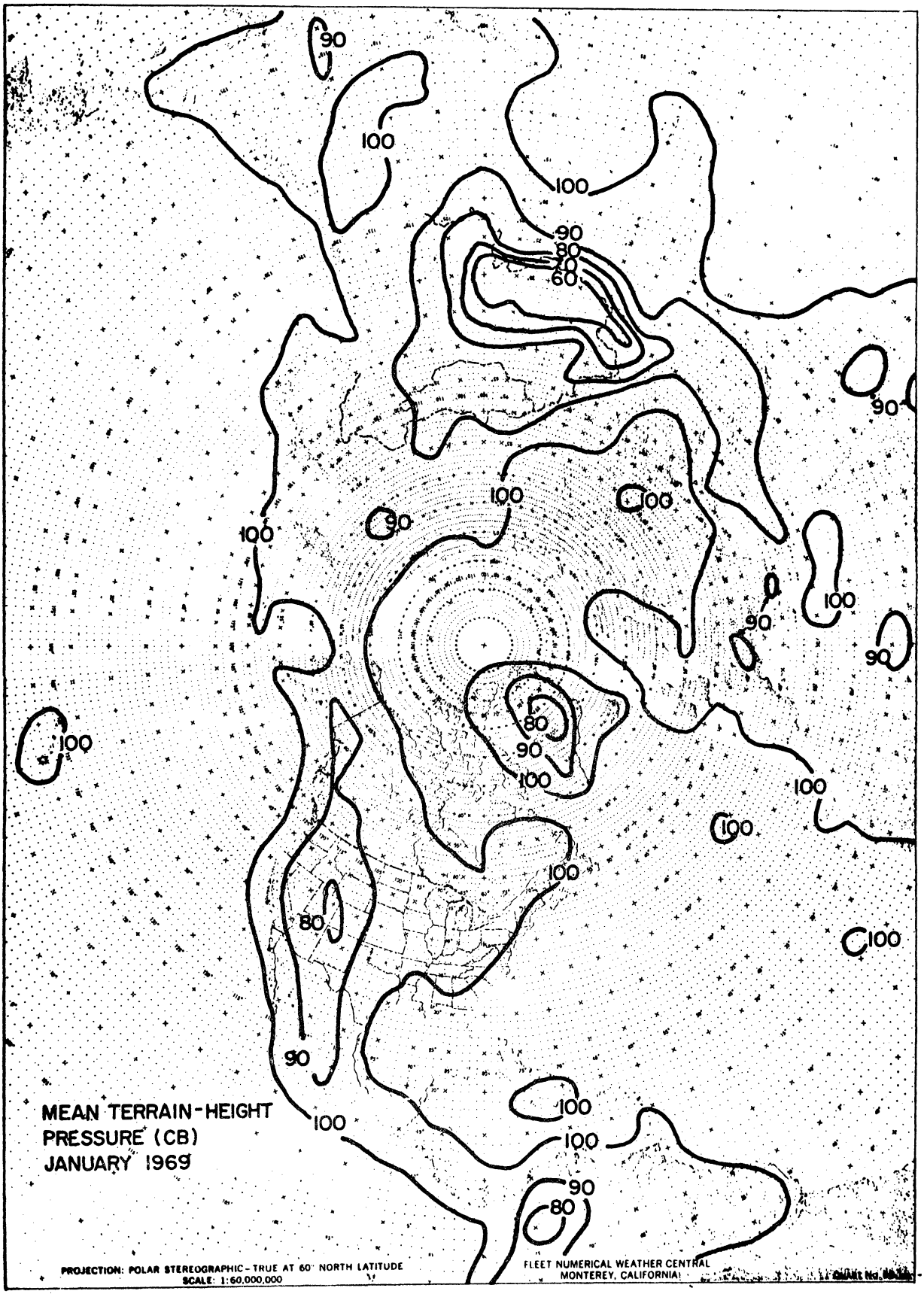

Fig. 21. Mean terrain-height pressure for January 1969.

A.7. TEMPERATURE AT TERRAIN HEIGHT

By definition, the specific temperature anomaly is

$$ST = \frac{T - T_p}{T_p} \quad . \tag{14}$$

Since the standard temperature at a given pressure level is calculated from

$$T_p = 288. - 6.5 \times 10^{-3} \cdot Z_p \quad , \tag{15}$$

the temperature at terrain height is computed from

$$T_o = (288. - 6.5 \times 10^{-3} \cdot Z_{p_o})(1 + ST) \quad . \tag{16}$$

Figure 22 presents the mean of the daily computations.

A.8. GEOSTROPHIC SURFACE WIND

The geostrophic surface wind can be represented by

$$\vec{V}_o = \vec{k} \times \frac{g}{f} (\nabla D)_o \quad . \tag{17}$$

Now the gradient of D at the terrain-height pressure requires the use of (10) but in this case Z_{p_o} is known. Letting the subscript op represent these values at terrain-height pressure, the geostrophic surface wind is determined from

$$V_o = \frac{mg}{2fd} \left[(D_{op,i+1,j} - D_{op,i-1,j})^2 + (D_{op,i,j+1} - D_{op,i,j-1})^2 \right]^{\frac{1}{2}} \quad . \tag{18}$$

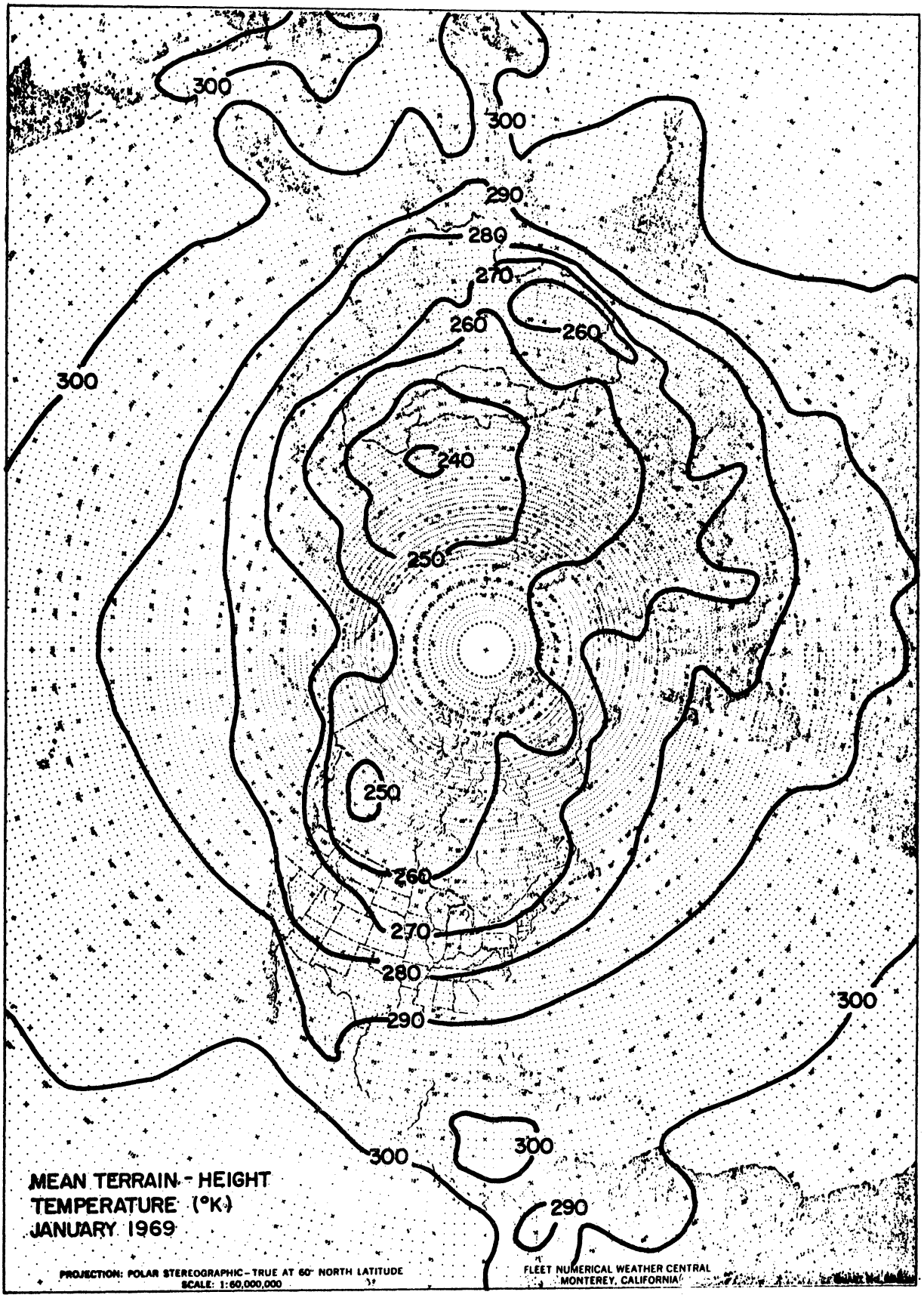

Fig. 22. Mean terrain-height temperature for January 1969.

A.9. GEOSTROPHIC SURFACE VORTICITY

From the same considerations used to obtain (18), the geostrophic surface vorticity can be computed from

$$\zeta_o = \frac{gm^2}{fd^2} \nabla^2 D_{op} \quad . \tag{19}$$

A.10. FRICTION EFFECTS, (2.15)

Combining (13), (16), (17), and (18), the frictional effects are computed from

$$\left(\frac{\partial F_y}{\partial x} - \frac{\partial F_x}{\partial y}\right)_o = \frac{g^3 m^3 p_{o,i,j}}{2f^2 d^3 \Delta p RT_{o,i,j}} [\,]^{\frac{1}{2}} \nabla^2 D_{op} \quad , \tag{20}$$

where the brackets contain the terms inside the brackets in (18).

A.11. OMEGA IN THE LOWER BOUNDARY, (2.19), (2.20)

The omega due to terrain is calculated using a form similar to (7) using the geostrophic surface wind. Calculating the omega due to friction is just a matter of multiplying (20) by $-\Delta p/f$.

A.12. HEATING AT THE LOWER BOUNDARY, (2.17)

Computing the lower boundary heating is straightforward using (13), (16), (17), and the vertical velocities. All the terms are averaged over the 24-hr period since the local time change term is also involved. The averaging is done using the form given in Section A.3.

BIBLIOGRAPHY

Berkofsky, L. and E. Bertoni, 1955: Mean Topographic Charts for the Entire Earth. Bull. Amer. Meteor. Soc., 36, No. 7, 350-354.

Brown, J. A., 1964: A Diagnostic Study of Tropospheric Diabatic Heating and the Generation of Available Potential Energy. Tellus, 16, No. 3, 371-387.

Burger, A. P., 1958: Scale Consideration of Planetary Motions of the Atmosphere. Tellus, 10, No. 2, 195-205.

Charney, J. G., 1948: On the Scale of Atmospheric Motions. Geofys. Publ., 17, No. 2, 1-17.

Clarke, L. C. and G. E. Lawniczak, Jr., 1962: Hemispheric Solution of the Omega Equation Including Terrain and Surface Frictional Effects. M. S. Thesis, U. S. Naval Postgraduate School, Monterey, Calif., 172 pp.

Cressman, G. P., 1960: Improved Terrain Effects in Barotropic Forecasts. Mon. Wea. Rev., 88, No. 9-12 327-342.

Dickson, R. R. and J. Posey 1967: Maps of Snow-Cover Probability for the Northern Hemisphere. Mon. Wea. Rev. 95, No. 6, 347-353

Dutton, J. A. and D. R. Johnson, 1967: The Theory of Available Potential Energy and a Variational Approach to Atmospheric Energetics. Advan. Geophys., 12, 333-436.

Gates, W. L., 1960: Static Stability Measures in the Atmosphere. Department of Meteorology, University of California, Los Angeles, p. 9.

Haltiner, G. J., L. C. Clarke, and G. E. Lawniczak, Jr., 1963: Computation of the Large Scale Vertical Velocity. J. Appl. Meteor., 2, No. 2, 242-259.

Haurwitz, B., 1941: Dynamic Meteorology, McGraw Hill, New York, p. 241.

Holl, M. M., J. P. Bibbo, and J. R. Clark, 1963: Linear Transforms for State-Parameter Structure. Tech. Memo. No. 1, Second Edition, Meteorology International, Monterey, Calif., 28 pp.

Johnson, D. R. and W. C. Shen, 1968: Profiles of Infrared Irradiance and Cooling Through a Jet Stream. Mon. Wea. Rev., 96, No. 8, 559-572.

Katayama, A., 1967: On the Radiation Budget of the Troposphere over the Northern Hemisphere (III)—Zonal Cross-Section and Energy Consideration. J. Meteor. Soc. Japan, 45, 26-38.

Kung, E. C., 1966: Kinetic Energy Generation and Dissipation in the Large-Scale Atmospheric Circulation. Mon. Wea. Rev., 94, No. 2, 67-82.

Kung, E. C., 1967: Diurnal and Long-Term Variations of the Kinetic Energy Generation and Dissipation for a Five-Year Period. Mon. Wea. Rev., 95, No. 9, 593-606.

Lawniczak, G. E., Jr., 1969: On a Multi-Layer Analysis of Atmospheric Diabatic Processes and the Generation of Available Potential Energy. The University of Michigan. Technical Report 08759-5-T, 111 pp.

Lettau, H., 1954: A Study of the Mass, Momentum, and Energy Budget of the Atmosphere. Geophys. Bioklimatol., Ser. B, A7, 135-157.

Lettau, H., 1959: Wind Profile, Surface Stress, and Geostrophic Drag Coefficients in the Atmospheric Surface Layer. Advan. Geophys., 6, p. 243.

Lorenz, E. N., 1955: Available Potential Energy and the Maintenance of the General Circulation. Tellus, 7, No. 2, 157-167.

Lorenz, E. N., 1967: The Nature and Theory of the General Circulation of the Atmosphere. World Meteorological Organization, 161 pp.

Manabe, S., J. Smagorinsky, and R. Strickler, 1965: Simulated Climatology of a General Circulation Model with a Hydrologic Cycle. Mon. Wea. Rev., 93, No. 12, 769-798.

Manabe, S. and J. Smagorinsky, 1967: Simulated Climatology of a General Circulation Model with a Hydrologic Cycle (II)—Analysis of the Tropical Atmosphere. Mon. Wea. Rev., 95, No. 4, 155-169.

Manabe, S. and B. Hunt, 1968: Experiments with a Stratospheric General Circulation Model. Mon. Wea. Rev., 96. No. 8, 477-539.

Oort, A. H., 1964: On Estimates of the Atmospheric Energy Cycle. Mon. Wea. Rev., 92. No. 11, 483-493.

Oort, A. H., 1964a: On the Energetics of the Mean and Eddy Circulations in the Lower Stratosphere. Tellus, 16, No. 4, 309-327.

Palmén, E. and C. W. Newton, 1969: Atmospheric Circulation Systems. Academic Press, p. 48.

Perry, J. S., 1967: Long-Wave Energy Processes in the 1963 Sudden Stratospheric Warming. J. Atmos. Sci., 24, No. 5, 539-550.

Phillips, N. A., 1963: Geostrophic Motion. Rev. Geophys., 1, No. 2, 123-176.

Sellers, W. D., 1965: Physical Climatology. The University of Chicago Press, p. 5.

Smagorinsky, J., S. Manabe, and J. L. Holloway, 1965: Numerical Results from a Nine-Level General Circulation Model of the Atmosphere. Mon. Wea. Rev., 93, No. 12, 727-768.

Wagner, A. J., 1969: The Weather and Circulation of January 1969—Continued Strong High-Latitude Blocking and Flood-Producing Rains in California. Mon. Wea. Rev., 97, No. 4, 351-358.

Wiin-Nielsen, A., 1959: On Certain Integral Constraints for the Time-Integration of Baroclinic Models. Tellus, 11, No. 1, 45-59.

Wiin-Nielsen, A. and J. A. Brown, 1960: On Diagnostic Computations of Atmospheric Heat Sources and Sinks and the Generation of Available Potential Energy. Proceedings of the International Symposium on Numerical Weather Prediction in Tokyo, Meteor. Soc. Japan, 593-613.

Wiin-Nielsen, A., 1967: On the Annual Variation and Spectral Distribution of Atmospheric Energy. Tellus, 19, No. 4, 540-559.

Wiin-Nielsen, A., 1968: On the Intensity of the General Circulation of the Atmosphere. Rev. Geophys., 6, No. 4, 559-579.